Optical Materials: X 25 (2025) 100390

Contents lists available at ScienceDirect

Optical Materials: X

journal homepage: www.journals.elsevier.com/optical-materials-x

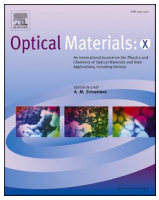

Evolution of phase composition and luminescent characteristics of the $La_{1-x-y}Sm_xCa_yVO_{4-\delta}$ nanocrystalline phosphor

S.G. Nedilko [a,*], O. Chukova [a,b], A. Dorofieieva [a], S.A. Nedilko [a], V. Shcherbatskyi [a], T. Voitenko [a], M. Etter [b], H.S. Rahimi Mosafer [c], W. Paszkowicz [c], Y. Zhydachevskyy [c], A. Suchocki [c]

[a] Taras Shevchenko National University of Kyiv, Volodymyrska Str., 64/13, Kyiv, 01601, Ukraine
[b] Deutsches Elektronen-Synchrotron (DESY), Notkestr. 85, Hamburg, 22607, Germany
[c] Institute of Physics, Polish Academy of Sciences, Al. Lotnikow 32/46, Warsaw, 02-668, Poland

ARTICLE INFO

Keywords:
Lanthanum vanadate
Phase composition
Crystal structure
Luminescence
Sm^{3+} ions

ABSTRACT

This work aims to clarify the relationship between the optical, particularly luminescent, characteristics of the $La_{1-x-y}Sm_xCa_yVO_{4-\delta}$ powder nanosized compounds with their phase composition and concentration of dopants. According to the high-accuracy XRD data, the samples are a mixture of monoclinic and tetragonal crystal phases. The diffuse reflection and photoluminescence (PL) spectra were measured and analyzed including spectral distributions and intensity ratios of the PL bands, the positions and half-widths of envelopes of the groups of lines in the PL spectra of Sm^{3+} ions. Estimated from the diffuse reflection data the band gap values are 3.85, and 3.82, 3.75, 3.78 eV for the samples with x = 0.1, y = 0, and (x, y) = 0.05, 0.10, 0.15, respectively. The PL excitation spectra of the $La_{1-x-y}Sm_xCa_yVO_{4-\delta}$ nanoparticles consist of both the wide UV wavelength band (260–360 nm) caused by transition in the VO_4^{3-} molecular groups and in a set of narrow lines caused by inner *f-f* transitions in the Sm^{3+} ions (spectral range 350–520 nm). The PL spectra of the $La_{1-x-y}Sm_xCa_yVO_{4-\delta}$ nanoparticles contain four groups of lines (I – IV) resulting from the $^4G_{5/2} \rightarrow {}^6H_{5/2}$, $^6H_{7/2}$, $^6H_{9/2}$, and $^6H_{11/2}$ transitions, respectively, in the inner *f* shell of the Sm^{3+} ions. The concentration behavior of the Sm^{3+} ions PL characteristics is related to the evaluation of the phase composition of $La_{1-x-y}Sm_xCa_yVO_{4-\delta}$ samples. It was found that the changes of the $R_{lum} = I_{(III)}/I_{(I)}$, where $I_{(III)}$ and $I_{(I)}$ are the integrated intensities of the corresponding groups of lines, can be related to the phase composition of the $La_{1-x-y}Sm_xCa_yVO_{4-\delta}$ compounds. Developed in this work the combined way of structural and optical data analysis may be useful in designing other multiphase phosphor systems containing Sm^{3+} ions.

1. Introduction

New effective luminescent materials (phosphors) are one of the important modern demands of optical material technology, as phosphors are used for the creation of new field emission displays, plasma display panels, electro-luminescent devices, solar cells, white light-emitting diodes, bio-markers, and bio-probes, etc. [1–10]. In many cases, phosphors comprise a matrix (host material) and some specially introduced luminescent dopant(s). Therefore, the selection of both luminescent dopant(s) and compatible host material is an important task in the development of new phosphors.

Lanthanide-based compounds are of wide use for phosphor development, as lanthanum ions can be easily replaced by many other rare earth (RE) luminescence ions due to the similarity of their ionic radius and electronic characteristics. A choice of the type of RE ions is determined by requirements of the areas of application of phosphors under development [5,6,8,11–14].

Lanthanide vanadates are promising for use as hosts for various applications because they are characterized by high chemical, thermal, ionizing irradiation stability, etc. It is also worth emphasizing that Lanthanide vanadates are of good choice as phosphor matrices, as they exhibit a high intensity of light absorption in the UV and near-UV range of light and high efficiency of excitation energy transfer from the host to the luminescent RE ions [6,10,15–18].

It should be noted that the Eu^{3+} ions were and remain the most popular among the RE ions used for the development of oxide-vanadate

* Corresponding author.
E-mail address: sgnedilko@gmail.com (S.G. Nedilko).

https://doi.org/10.1016/j.omx.2024.100390
Received 15 August 2024; Received in revised form 27 October 2024; Accepted 2 December 2024
Available online 9 December 2024

phosphors, in particular for the development of light-converting coatings for white light-emitting diodes (WLEDs) [19–25]. Much less attention was paid to studying vanadate crystals doped with samarium ions, despite the fact they have demonstrated efficient luminescence in the orange-reddish spectral range and a possibility of being excited with the near UV and violet light [26–28]. The last feature is important for phosphor-converted WLEDs [27–33].

There are several approaches to the development of phosphor coatings for WLEDs which allow getting near white light. Some of these involve multi-component coatings, where each of the components emits light of one color: red, green, and blue, resulting in a white emission. Another way leads through the development of single-component coatings based on single-phase crystalline materials co-doped with several types of RE which also emit blue, green, and red light. Single-phase coatings are also being developed, the luminescence of which, combined with the radiation of an LED chip, can create light similar to white. A blue GaN/InGaN chip coated with a yellow emission YAG:Ce^{3+} phosphor is a commercial variant of the latter. Each of the mentioned approaches has some advantages and disadvantages, too. The main disadvantage of the single-component coatings is the difficulty of the single-phase composition controlling at the high concentration of a dopant(s) and, especially, in a case of co-doping with ions of various types [6,13,34,35], and elsewhere.

We consider that the requirement of a single-phase composition of a material may not be particularly strict. On the contrary, the structural multiphase composition in the case of chemically homogeneous powder material can be used in the development of new phosphors. The WLED's luminescent coverings are just the cases when the structural multiphase properties can be used to tune their optical, in particular, luminescent properties. For the development of such types of coatings, it is necessary to have clear data on the correlation of optical properties with the structural characteristics and phase composition of a material.

As a rule, when studying phosphors, a serious attention is paid to the relation between their structural and optical (luminescent) characteristics [36–41]. The effect of structural multiphase property was also considered in detail in the study of phosphors based on simple oxides, such as zirconia (ZrO_2), titania (TiO_2), etc. These compounds' phase composition can change, particularly under the influence of introduced dopants, including RE ions. It was found that the peculiarities of luminescence details, particularly of the Eu^{3+} dopant ions, can be used to monitor the phase stabilization effects. The number of lines in spectral multiplets, the ratio of the hypersensitive $^5D_0 \rightarrow {}^7F_2$ radiation transition intensity to the intensity of the $^5D_0 \rightarrow {}^7F_1$ radiation transition, as well as the changes of the $^5D_0 \rightarrow {}^7F_2$ transition main lines positions, are the luminescence spectral features which have been mainly used for noted monitoring [42–46]. The same characteristics of the Eu^{3+} ions PL were used to monitor to some degree the phases content in complex oxide phosphors [47–52].

It is obvious that if it is necessary to clarify the relationship between the phase composition and optical characteristics, then it is necessary to have detailed information about the composition and structure of the studied system. First, reliable data on the content of various phases in the composition of the material are necessary. Secondly, the optical characteristics of the materials selected for such studies should be sensitive to structural and phase transformations and at the same time be available for measurements and analysis.

An opportunity to use such an approach is shown in this work on a comprehensive study of a series of samples of lanthanum orthovanadate $LaVO_4$ doped with Sm^{3+} ions and co-doped with Ca^{2+} ions. Lanthanum orthovanadate was used as a matrix, because its phase composition can be changed from monoclinic to tetragonal phase (in other words, from monazite to zircon type structure) by introducing alkaline earth (Ca^{2+}, Ba^{2+}, …) and some other, in particular RE ions, dopants [52–57]. The Sm^{3+} ion was selected as the luminescent activator taking into account the above-mentioned prospects of practical application of phosphors containing this ion, and the possibility of using it as a luminescent probe sensitive to the symmetry and strength of the crystal field in its nearest surrounding. Absorption and PL bands caused by hypersensitive transitions in the Sm^{3+} ions are observed in the range of visible light, which ensures their reliable registration. Our previous experience in studying the effect of Ca^{2+} ions on the structural and luminescent properties of lanthanum orthovanadate $LaVO_4$ doped with Eu^{3+} and Er^{3+} ions [51,56], as well as excellent luminescent characteristics of the $La_{1-x}Sm_xVO_4$ nanosized powders prepared and studied by us before [32] were also important factors in choosing the noted object of study.

Thus, the purpose of this work is to clarify the relationship between the optical, mainly luminescent, characteristics of the $La_{1-x-y}Sm_xCa_yVO_{4-\delta}$ compound with its phase composition and concentration of dopants which initiate structural phase transformations. To achieve the goal, the phase composition of the mentioned samples was determined by the XRD method using various modern equipment. The optical absorption (diffuse reflection) spectra and the main photoluminescence (PL) characteristics were measured (spectral distributions and intensity ratio of the bands in the PL excitation spectra; positions and half-widths of envelopes of groups of narrow luminescence lines of the Sm^{3+} dopant ions and their intensity ratios, etc.). The $La_{1-x-y}Sm_xCa_yVO_{4-\delta}$ sol-gel nanoparticles were synthesized and studied in the noted context for the first time. It is expected that the obtained results can be useful for the engineering of optical (mainly, luminescent) characteristics of various types of oxide compounds doped with Sm^{3+} ions. In particular, this could be done by using of the received data sets in special computer simulation programs [58].

2. Samples, experimental equipment and procedures

The $La_{1-x-y}Sm_xCa_yVO_{4-\delta}$ nanoparticles were obtained by a citrate-nitrate sol-gel synthesis. The δ variable in this formula takes into account the charge compensation needed due to the replacement of RE^{3+} ions by Ca^{2+} ions. It is known that such replacement leads to an increased concentration of oxygen vacancies in a crystalline lattice. Nitrate solutions of lanthanum (III), samarium (III), and calcium (II) oxides, ammonium metavanadate, ammonium hydroxide, citric acid, and nitric acid were used for synthesis. The details of the synthesis of such type of materials have been published in our previous works [32,51]. The applied nominal concentrations of the dopants were 5, 10, 15, and 20 mol % (x; y = 0.05, 0.1, 0.15, 0.2).

X-ray diffraction (XRD) patterns were taken using a Philips X'Pert Pro Alpha1 diffractometer operating in Bragg-Brentano geometry and working in continuous scanning mode using CuKα radiation. These data were collected in steps of 0.0167° in the range of 14°–158.9° (2θ) (Below, in Table 1 they are marked as Lab. data.). High-resolution X-ray powder diffraction measurements were also performed at PETRA III Beamline P02.1 at DESY using a synchrotron radiation beam with 0.0207518 nm wavelength. The data were collected at room temperature with the step of 0.003149° in the range of 0.0239°–15.7431° (2θ) (Below, in Table 1 they are marked as Synchr. data.). Rietveld refinements were performed using the FullProf program [59]. The evaluation of different phases mass percentage was also performed from the Rietveld refinement procedure.

The microstructure of the samples and chemical elements distribution were studied using Scanning Electron Microscopy (SEM) and Energy Dispersive Spectroscopy (EDS) tools at INCA X-max System from Oxford Instruments. Diffuse reflection spectra of the samples were measured with a PerkinElmer Lambda 950 spectrometer. Luminescence emission spectra were excited with 325, 405, and 473 nm lasers or a powerful Xenon lamp and registered with a DFS-12 spectrometer and a FEU-79 photomultiplier. Excitation spectra were measured using DMR-4 and DFS-12 spectrometers and a FEU-79 photomultiplier [3,32]. Some of the luminescence measurements were performed at liquid helium (4.2 K) temperature to find out more details on the structure of the luminescence centers. The emission intensity was evaluated as an integral (area under the spectral curve) in a certain spectral range.

Table 1
Phase composition and crystallographic of the $La_{1-x-y}Sm_xCa_yVO_{4-\delta}$ unit cell parameters.

	Space group	Percentage of each phase (wt%)	*a* (Å)	*b* (Å)	*c* (Å)	*β*	*V*(Å^3)	Ref.
$La_{0.9}Sm_{0.05}Ca_{0.05}VO_{4-\delta}$	$P2_1/n$	97.8(2)	7.03275 (6)	7.26980(6)	6.72150 (5)	104.9208(4)	332.064 (5)	Lab. data
	$I4_1/amd$	2.23(2)	7.3999(3)	7.3999(3)	6.4967(5)	90	355.75(3)	
$La_{0.8}Sm_{0.1}Ca_{0.1}VO_{4-\delta}$	$P2_1/n$	73.7(3)	7.03548 (9)	7.27251 (9)	6.72157 (9)	104.89619 (74)	332.355 (7)	Lab. data
	$I4_1/amd$	22.2(1)	7.3914 (1)	7.3914(1)	6.4905(1)	90	354.59 (1)	
	$C12/m1$ (CaV_2O_6)	4.1(2)	10.072 (2)	3.6700(5)	7.039 (1)	104.88(1)	251.47 (7)	
$La_{0.7}Sm_{0.15}Ca_{0.15}VO_{4-\delta}$	$P2_1/n$	12.82(9)	7.0346(4)	7.2707 (4)	6.7228(4)	104.926 (5)	332.25(3)	Lab. data
	$I4_1/amd$	84.1(3)	7.40207 (8)	7.40207 (8)	6.50031 (8)	90	356.156 (7)	
	$C12/m1$ (CaV_2O_6)	3.1(1)	10.0664(6)	3.6709(2)	7.0365(5)	104.803(5)	251.39(3)	
$La_{0.7}Sm_{0.15}Ca_{0.15}VO_{4-\delta}$	$P2_1/n$	12.9(1)	7.0283(8)	7.2652(7)	6.7179(7)	104.92016	331.46(6)	Synchr. data
	$I4_1/amd$	80.4(5)	7.3994(2)	7.3994(2)	6.4978(2)	90	355.76(1)	
	$C12/m1$ (CaV_2O_6)	6.8(3)	10.094(5)	3.6602(2)	6.700(4)	104.80 (4)	250.0 (2)	
$La_{0.6}Sm_{0.2}Ca_{0.2}VO_{4-\delta}$	$I4_1/amd$	90.9(4)	7.37960 (9)	7.37960 (9)	6.48194 (9)	90	352.997 (8)	Lab. data
	$C12/m1$ (CaV_2O_6)	9.1(2)	10.0713(7)	3.6724(2)	7.0345 (5)	104.782(5)	251.57(3)	
$La_{0.6}Sm_{0.2}Ca_{0.2}VO_{4-\delta}$	$I4_1/amd$	87.2 (6)	7.3763(2)	7.3763(2)	6.4792 (2)	90	352.54 (2)	Synchr. data
	$C12/m1$ (CaV_2O_6)	12.8(4)	10.084(3)	3.65(1)	7.025(2)	105.03 (2)	250.2 (1)	
$LaVO_4$	$P2_1/n$	100	7.047(1)	7.286(1)	6.725(1)	104.85(1)	333.76	[60]
$LaVO_4$	$I4_1/amd$	100	7.4578(7)	7.4578 (7)	6.5417 (9)	90	363.84	[62]
$SmVO_4$	$I4_1/amd$	100	7.2647(9)	7.2647 (9)	6.384(1)	90	336.92	[61]
CaV_2O_6	$C12/m1$	100	10.060(2)	3.673(1)	7.038(2)	104.8(1)	251.43	[63]

3. Experimental results

3.1. XRD data analysis

Phase analysis of the synthesized $La_{1-x-y}Sm_xCa_yVO_{4-\delta}$ compounds showed that they contain two phases and each sample is a mixture of monazite and zircon-type structures, except (x, y) = 0.2 (zircon only). By increasing the amount of Sm and Ca the samples tend to change from monazite-to zircon-type structure (Fig. 1 and Fig. S1). Samples with (x, y) = 0.1, 0.15, and 0.2 contain also a low amount of CaV_2O_6 phase.

The refinement involved the zircon and monazite-type phases in each sample. The applied models include also the minority phase (CaV_2O_6). For the first two samples, a structural model for the refinement was taken from $LaVO_4$ [60] (ICSD code: 400) with space group $P2_1/n$ and for the last two samples, $SmVO_4$ [61] with space group $I4_1/amd$ (ICSD code: 81701) was selected as a starting model. The resulting values of lattice parameters, volume, and percentage of each phase are accumulated in Table 1. The main phase of the $La_{0.9}Sm_{0.05}Ca_{0.05}VO_{4-\delta}$ and $La_{0.8}Sm_{0.1}Ca_{0.1}VO_{4-\delta}$ is of monazite-type (monoclinic structure) with less than 22 % of zircon-type (tetragonal structure), whereas the main phase of the $La_{0.7}Sm_{0.15}Ca_{0.15}VO_{4-\delta}$ is of zircon-type with less than 13 % of monazite-type phase. There is no trace of a monoclinic phase in the $La_{0.6}Sm_{0.2}Ca_{0.2}VO_{4-\delta}$.

The unit cell variation with the substitution of Sm and Ca ions can be explained by the differences in the ionic radii of La and noted two ions. The ionic radii of La^{3+}, Sm^{3+}, and Ca^{2+} ions have been reported to be 1.216 Å (CN = 9), 1.132 Å (CN = 9), and 1.18 Å (CN = 9), respectively [64]. By evaluation of the unit-cell volume it can be understood that the monazite-type phase is enriched with La, otherwise, the zircon structure type is enriched with Sm and Ca. For the last two samples with zircon-type structure, the unit cell volume decreases by adding Sm and Ca in comparison to $LaVO_4$ ($I4_1/amd$).

A good example of the concentration dependence of unit-cell parameters by doping rare earth and divalent ions in the monazite-type crystal structure was found for $LaVO_4$:Yb^{3+}/Ln^{3+}, M^{2+} [65]. By doping rare earth ions such as Sm^{3+}, Ho^{3+}, and Er^{3+} the phase structure of the host lattice ($LaVO_4$, monazite-type) remains unchanged [66]. There is not much difference in the unit cell volume (less than 1 %) of CaV_2O_6 with the reported one and it is less probable that La or Sm can enter to this secondary phase.

For $La_{0.8}Sm_{0.1}Ca_{0.1}VO_{4-\delta}$, the vertical upper bar is $La_{0.8}Sm_{0.1}Ca_{0.1}VO_{4-\delta}$ with space group P21/n, middle is $La_{0.8}Sm_{0.1}Ca_{0.1}VO_{4-\delta}$ with space group $I4_1/amd$, and lower is CaV_2O_6. For $La_{0.6}Sm_{0.2}Ca_{0.2}VO_{4-\delta}$ the vertical upper bar is $La_{0.6}Sm_{0.2}Ca_{0.2}VO_{4-\delta}$ with space group $I4_1/amd$ and lower is CaV_2O_6

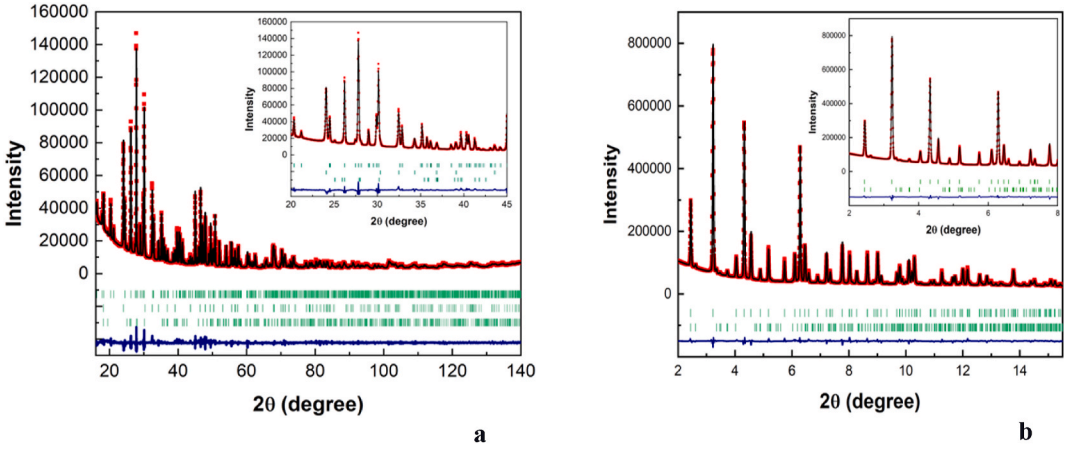

Fig. 1. Rietveld refinement of the a) $La_{0.8}Sm_{0.1}Ca_{0.1}VO_{4-\delta}$ (R_P = 3.55, R_{WP} = 4.78) and b) $La_{0.6}Sm_{0.2}Ca_{0.2}VO_{4-\delta}$ (R_P = 2.86, R_{WP} = 4.30) samples. Red squares represent the experimentally observed X-ray diffraction profiles of the respective samples, whereas the solid black line corresponds to the calculated X-ray diffraction patterns and the deviation of the theoretical data from the experimental values is shown by a blue line at the bottom. The green vertical bars represent the Bragg reflection positions.

3.2. Morphology of the samples

The $La_{1-x-y}Sm_xCa_yVO_{4-\delta}$ powders consist of different particles whose sizes vary mainly between 100 and 400 nm (Fig. 2). These particles can be grouped, especially at low dopant concentration, into lumps of irregular shape (Fig. 2a and b). The samples with low dopant concentrations (x, y) = 0.05 and 0.1 contain nanoparticles at least of two different types shapes, and sizes. Those of type 1 are elongated with a rectangular basis; those of type 2 are of rounded shape (Fig. 2b). Samples with a higher dopant concentration (x, y = 0.15 and especially 0.2) are characterized by a uniform shape of particles (Fig. 2c and d).

If these results to compared with the XRD data, it should be concluded that the heterogeneity of the shapes and sizes of the particles shown in Fig. 2a and b is related to the presence of particles belonging to both the tetragonal and the monoclinic phases, while the homogeneity of the shape of the particles shown in Fig. 2d correspond to the particles of the tetragonal phase of the orthovanadate. Besides, it should be noted that only the samples with a high amount of the monoclinic phase contain larger particles (Fig. 2a and b), while the samples with high content of tetragonal phase (Fig. 2d) are characterized with smaller sizes and higher packing density of the particles, and therefore by a larger area of their contacts. So, the observed shapes and sizes correlate with the phase composition, and we attribute the type 1 shape to the monoclinic phase, and the type 2 – to the tetragonal phase.

3.3. Diffuse reflection spectra

The measured diffuse reflection spectrum of the $La_{1-x-y}Sm_xCa_yVO_{4-\delta}$ nanoparticles not doped with calcium is characterized by a reflection coefficient of 80–90 % in the spectral range from 550 to 800 nm (Fig. 3, curve 1). For the samples of this type a smooth reflection edge is observed in the range of about 350 nm (Fig. 3). A set of narrow lines is also observed on the background of the noted reflection edge in the range of 360–500 nm. The peaks of the lines are at 360, 364, 374, 380, 404, 422, 434, 442, 460, 466, 478, 490, and 502 nm. The more

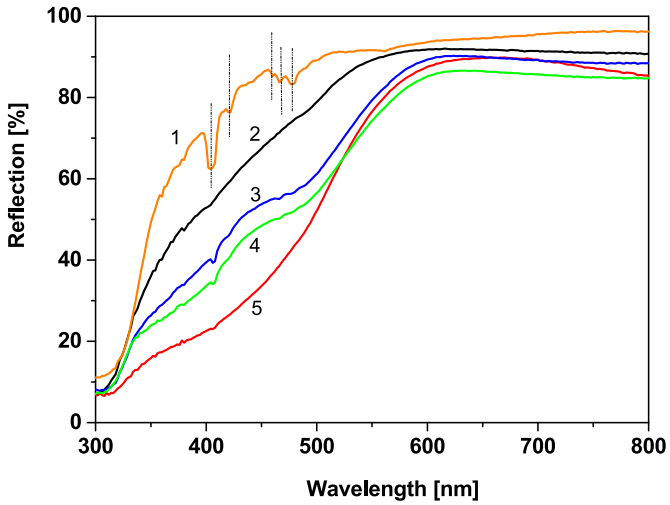

Fig. 3. Diffuse reflection spectra of the $La_{0.8}Sm_{0.2}VO_4$ (1) and $La_{1-x-y}Sm_xCa_yVO_{4-\delta}$ samples (2–5); (x, y) = 0.05 (2), 0.1 (3), 0.15 (4), and 0.2 (5); T = 300 K.

distinguished of them (404, 422, 460, 466, and 478 nm) are marked with dashed lines in Fig. 3.

The introduction of the Ca dopant leads to the appearance of a broad absorption band located in the range from 350 to 470 nm. It can be supposed that the band consists of at least two components with maximums near 400 and 500 nm. The intensity of these absorption bands increases with dopant concentrations increasing (Fig. 3, curves 2–5).

3.3.1. Luminescence properties: emission spectra

Luminescence spectra of the $La_{1-x-y}Sm_xCa_yVO_{4-\delta}$ nanoparticles at room temperature of the samples consist of four groups of lines in a 525–725 nm spectral range (marked here and after as groups I – IV, Fig. 4). These groups are located in the ranges of 525–580 (group I),

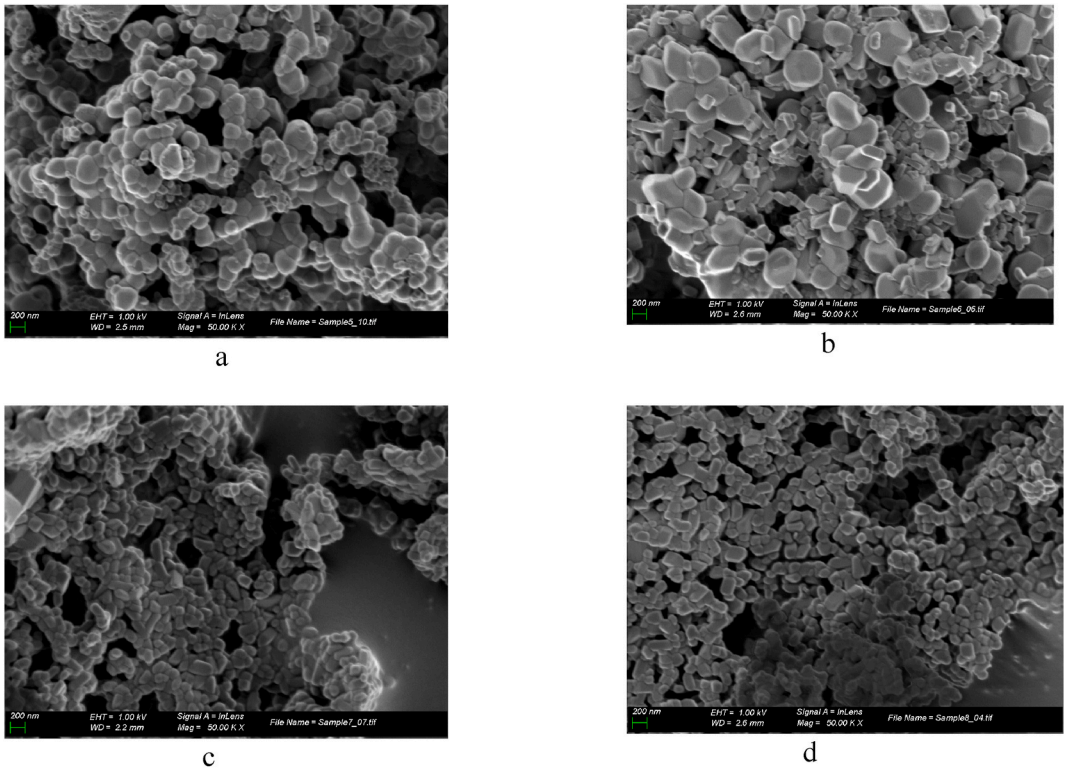

Fig. 2. SEM images of the $La_{1-x-y}Sm_xCa_yVO_{4-\delta}$ powders; (x, y) = 0.05 (a), 0.1 (b), 0.15 (c), and 0.2 (d).

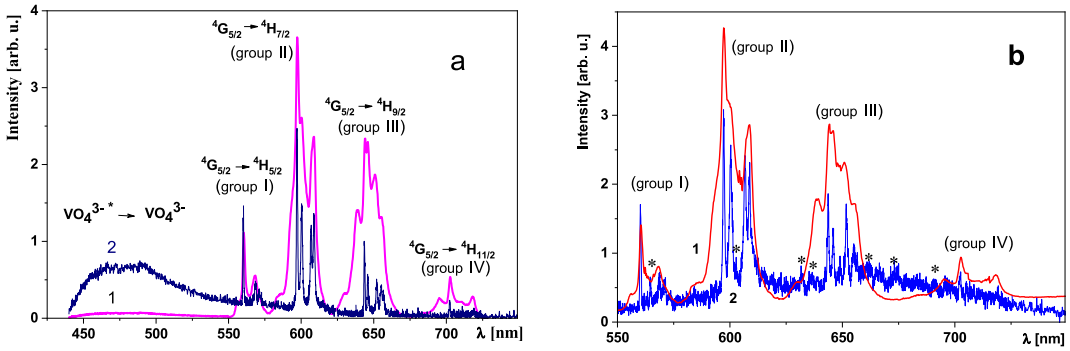

Fig. 4. The PL spectra of $La_{0.9}Sm_{0.1}VO_4$ (a) and $La_{0.8}Sm_{0.1}Ca_{0.1}VO_{4-\delta}$ samples (b); T = 300 (1), and 4.2 K (2); λ_{ex} = 405 nm.

580–620 (group II), 620–675 (group III) and 675–725 nm (group IV). A decrease of temperature leads to the narrowing of the lines which become less overlapping and, as a result, the spectral components are separated (Fig. 4, curves 2). The short-wave components in each of the groups disappear when the temperature decreases. The positions of the lines in these four groups are collected in Table S1.

The described linear spectra are observed on the background of broad emission bands covering the ranges of 425–550 and 500–750 nm if temperatures of the $La_{0.9}Sm_{0.1}VO_4$ samples are lowered and short-wave excitation (310–405 nm) is used (Fig. 4, curve 2). The intensity of the broad bands falls by at least 10 times if the temperature increases from 4.2 K to room temperature. The maxima of these bands are located (according to a rough estimation) around 475 ± 10 and 600 ± 10 nm.

Doping with calcium ions practically does not change the shapes of the PL spectra of the $La_{0.9}Sm_{0.1}VO_4$ sample at room temperature (Fig. 4b, curve 2), however, it suppresses the short-wavelength emission band, and additional lines of low intensity can be observed in each of the groups of the linear spectra (These lines are marked with esters in Fig. 4b, curve 2 and in Table S1.). The positions of all the PL lines in the spectra of the $La_{0.8}Sm_{0.1}Ca_{0.1}VO_{4-\delta}$ sample at T = 300 and 4.2 K (λ_{ex} = 405 nm) are also accumulated in Table S1.

3.3.2. *Luminescence properties: excitation spectra*

Excitation spectra of the $La_{1-x-y}Sm_xCa_yVO_{4-\delta}$ samples were measured at the PL lines λ_{reg} = 597, and 645 nm, which correspond to the most intensive groups in the linear emission spectra. Excitation spectra measured at λ_{reg} = 597 nm at 300 K consist of both a wide short wavelength band in 275–350 nm spectral range with maximum near 325 nm and narrower long wavelengths bands in 350–390, 390–440, and 450–520 nm spectral ranges with peak positions near 375, 400, and 468 nm, respectively (Fig. 5a). The noted components are structured and one can see two components both in the ranges of 350–390, and 390–440 nm. Peak positions of noted components are near 365 and 375 nm for the first range and 400, 415 nm for the 390–440 nm range.

When the temperature decreases to 4.2 K, the maximum of the wide excitation band shifts to shorter wavelengths ($\lambda_{max} \approx$ 310 nm), and the long-wavelength bands split into several narrow lines with positions around 342, 359, 373, 387, 394, 400, 410, 435, 440, 448, 458, 468, 473, 476, and 481 nm. The intensity of such a long-wave excitation essentially falls with the decrease of temperature if compared with the intensity of the wide short-wave excitation band.

Contrary to the emission spectra, excitation spectra of the $La_{0.8}Sm_{0.1}Ca_{0.1}VO_{4-\delta}$ Ca-doped samples differ from the spectra of the Ca-free $La_{0.9}Sm_{0.1}VO_4$ samples even at room temperature. In particular, the wide short wavelength excitation band for the $La_{0.8}Sm_{0.1}Ca_{0.1}VO_{4-\delta}$ is more intensive compared to the long wavelength range of the excitation spectrum, and its maximum is located at 317 nm (Fig. 5b).

A decrease of the $La_{0.8}Sm_{0.1}Ca_{0.1}VO_{4-\delta}$ temperature to 4.2 K causes changes similar to those observed in the above-described samples without calcium (Fig. 5b, curve 2). The long wavelength bands at 4.2 K are located at 342, 359, 372, 386, 394, 401, 413, 434, 448, 458, 468, 472, 476, and 481 nm. Taking into account the inaccuracy in the evaluation of peak positions caused by their shapes and overlapping, it can be assumed that Ca-doping does not cause shifts of the noted excitation bands (see data listed above).

The excitation spectra obtained at λ_{reg} = 645 nm are similar in terms of their structure and positions of the maxima to the spectra obtained at λ_{reg} = 597 nm, but the relative intensity of longer wavelength spectral components slightly differ from those shown in Fig. 5.

3.3.3. *Luminescence properties:concentration behavior*

For most practical applications, as well as for those stated in this work, data obtained for samples under ambient conditions are of large importance. Therefore, the spectral-luminescent properties of the $La_{1-x-y}Sm_xCa_yVO_{4-\delta}$ concentration series of the samples were studied just for room temperature, 300 K.

It was found that the luminescence characteristics of the studied samples depend on dopant concentration. The total intensity values

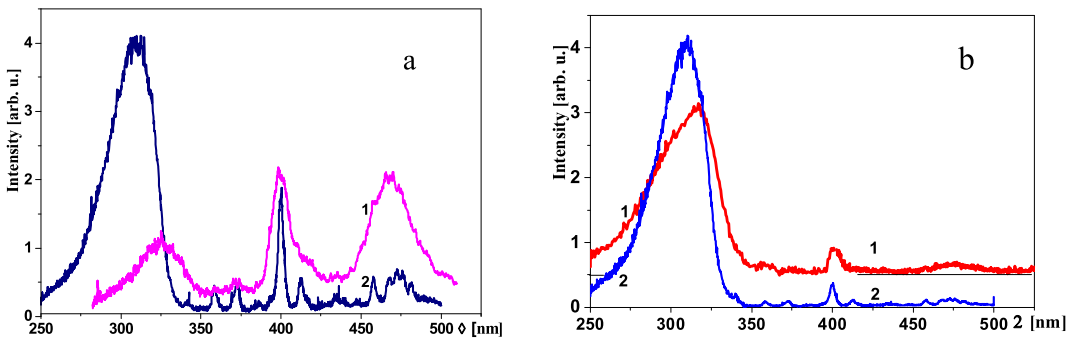

Fig. 5. Excitation spectra of $La_{0.9}Sm_{0.1}VO_4$ (a) and $La_{0.8}Sm_{0.1}Ca_{0.1}VO_{4-\delta}$ samples; λ_{reg} = 597 nm; T = 300 (1), and 4.2 K (2).

(I_{lum}(total)) were estimated as areas under spectral curves in the range of 525–725 nm. The intensity values for the spectral groups I and III were estimated as areas under spectral curves in the ranges of 525–580 and 620–675 nm, respectively. It was found that an increase of the dopant concentrations from y = 0.05 to y = 0.1 is accompanied by an increase of I_{lum}(total) by approximately 9 %. The next increase of dopant concentrations to y = 0.15 leads to a strong decrease of the total emission intensity by about 2.5 times, and after, the increase of dopant concentration up to the value of 0.2 is accompanied by an intensity increase by approximately 10 % (Fig. 6, curve 4).

The concentration behavior of the intensity of the I – IV groups, components of the PL spectra, is similar to that described above. However, for these spectral details, the rates of intensity changes in the mentioned concentration ranges are somewhat different from those above noted (Fig. 7, curves 4–6).

We observed also that the ranges of slow and rapid changes in the intensity of the total luminescence and its components correspond to ranges of slow and rapid changes in the content of the monoclinic and tetragonal phases in the composition of the samples (see Fig. 6).

Besides noted changes, a redistribution of the intensity of the components inside of each of the groups of lines also takes place. In general, changes in the structure and intensity of the lines can be characterized as a simplification of the structure and a narrowing of the Gaussian envelope of each of the groups (Table S2). The evaluation was not performed for groups I and IV, taking into account the low intensity of the emission in these ranges and the related inaccuracy as a result. However, for group I, it was possible to estimate the distance Δ between the main lines of the group (in Fig. 7a, they are indicated by short lines). It was found that Δ values significantly decrease (from ~220 to ~110 cm^{-1}) with dopant concentration increasing (Table S2).

The narrowing of other groups occurs mainly due to a decrease in the intensity of the sidelines in the group compared to the intensity of the lines located closer to the center. This is illustrated in Fig. 7a, where the components whose intensities decrease, are shown by downward arrows (their positions are 584, 597, and 609 nm), and the components whose relative intensities increase with the concentration of impurities increasing, are shown by arrows pointing up. It is noteworthy that in group II, the line of the highest intensity is peaked at 597 nm for the samples with a lower concentration of dopants (0.05 and 0.1), while for the samples with a higher concentration of dopants (0.15 and 0.2), the line of the highest intensity is peaked at 601 nm.

As for group III, the lines located at 640 and 654 nm should be attributed to lines that disappear when passing from the samples with a low content of impurities to the samples with a high content of impurities. On the contrary, the relative intensity of the line at 646 nm, increases and it dominates in the spectrum for the samples with a high content of dopants (x, y) = 0.15 and 0.2 (Fig. 7,a).

Similarly, it is possible to describe the behavior of the lines in the PL spectra measured at λ_{ex} = 473 nm (Fig. 7b). In Fig. 8b, as well as in Fig. 8a, the spectral components whose intensity decreases with an increase of dopants concentration are also shown by downward arrows, and the components whose relative intensity increases with an increase of dopants concentration are shown by upward arrows. The components of the first type have maximum positions at 561, and 569 nm (group I), 585, 598, 608, and 610 nm (group II), 630, 640, 647, 651, and 657 nm (group III). Components of the second type are located, in particular, at 564, 601, and 645 nm, for the groups I, II, and III, respectively.

Characteristics of the PL excitation spectra depend on the dopant concentrations in some manner, too. Thus, the main wide short wavelength band and its maximum shift to a shorter wavelength at around 5 nm if the impurity content increases from (x, y) = 0.05, and 0.1 to 0.15, and 0.2 (Fig. 8a). The shape of this band also changes if dopants are incorporated into the samples (Fig. 8b).

One can see also, that the dependence of the total intensity of the excitation spectra (I_{exc}(total)) measured in the 260–520 nm range is similar (Fig. 6c) to the concentration dependence of the luminescence

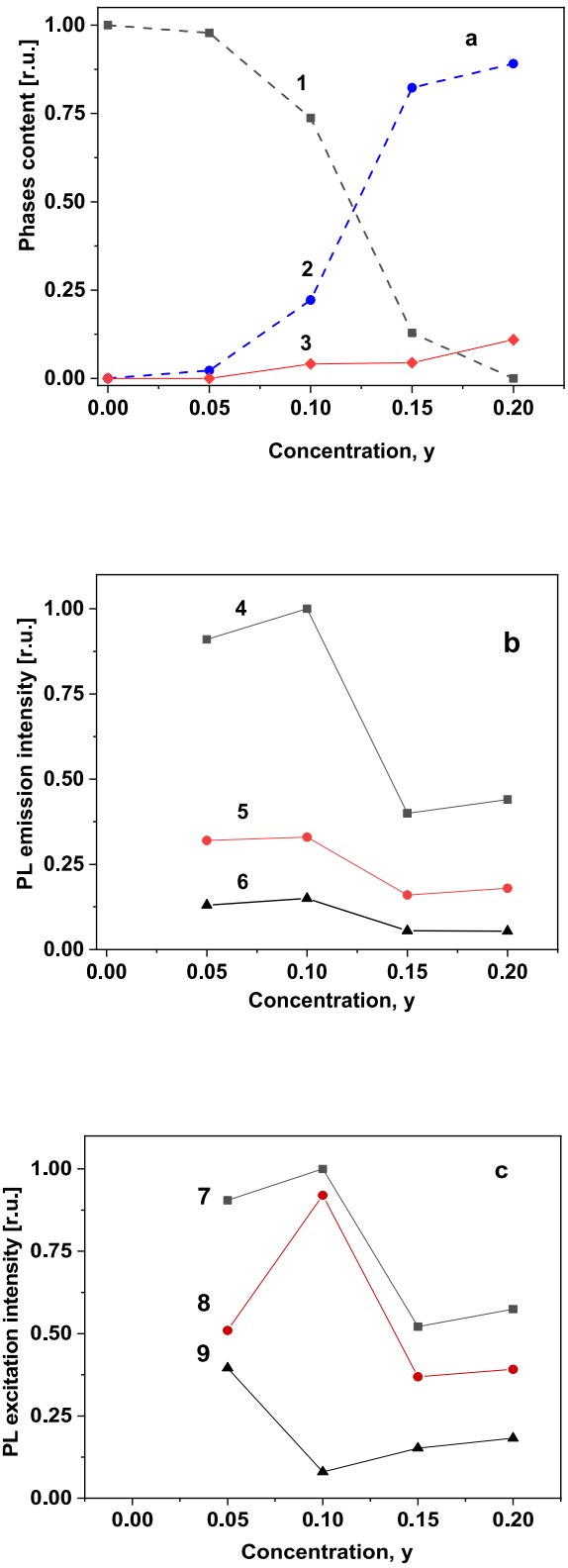

Fig. 6. The dependences of the: a) monoclinic C^m (1), tetragonal C^t (2), and impurity phase CaV_2O_6 (3) content; b) total luminescence intensity I_{lum}(total) (4), intensity of the PL group III (5), and intensity of the PL group I (6); c) total intensity of the luminescence excitation spectrum I_{exc}(total) (7), intensity of the luminescence excitation short wavelength band I_{short} (8), intensity of the luminescence excitation long wavelength band I_{long} (9) on the dopant concentrations (x, y) for the $La_{1-x-y}Sm_xCa_yVO_{4-\delta}$ samples; λ_{ex} = 325 nm (1 – 6); λ_{reg} = 597 nm (7–9).

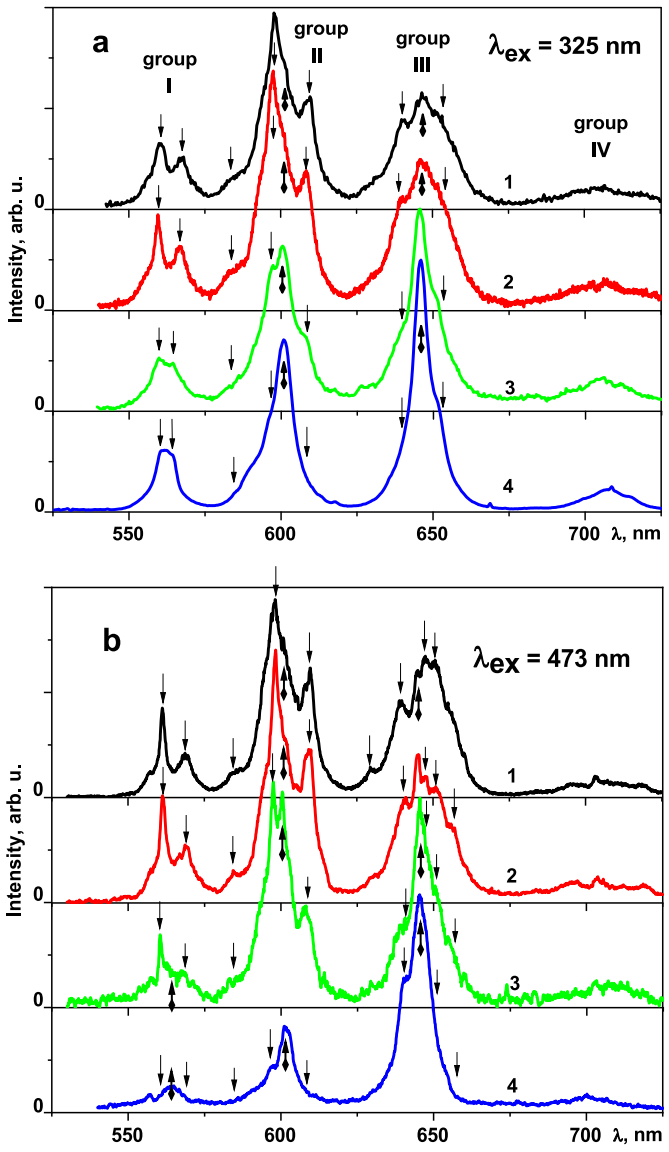

Fig. 7. Emission spectra of the $La_{1-x-y}Sm_xCa_yVO_{4-\delta}$ samples, (x, y) = 0.05(1), 0.1 (2), 0.15 (3), 0.2 (4); λ_{ex} = 325 (a) and 473 nm (b); T = 300 K.

intensity (Fig. 6b). At the same time, the behavior of the intensity of both the short-wavelength (I_{short}) (measured in the 260–360 nm range) and the long-wavelength parts of the excitation spectra (I_{long}) (measured in the 360–520 nm range) differ from the mentioned above (Fig. 6c, curves 8 and 9).

Concentration changes in the shape and intensity of excitation spectra registered in group III of the PL spectra (λ_{reg} = 645 nm) are similar to those described above for the case with λ_{reg} = 597 nm. The corresponding values of intensities (I_{exc}(total), I_{short}, and I_{long}) are accumulated in Table S2.

4. Discussion

The obtained XRD results are consistent with literature data on the lanthanum orthovanadate crystal lattice transformation from a monoclinic to a tetragonal crystal structure due to the introduction of two-charged dopants [51–57]. We have also found that the content of the tetragonal $LaVO_4$ phase increases when the concentrations of the Sm^{3+} and Ca^{2+} ions increase (Table 1). Concentration dependences of the monoclinic and tetragonal phases content on the *y* value in the $La_{1-x-y}Sm_xCa_yVO_{4-\delta}$ samples are also demonstrated in Fig. 6a. It should be noted, that the phase content changes are described by the fairly smooth curves 1–3 in the Figure. An increase of the *y* value from zero to 0.05 leads to an appearance of only 2.2 % of the tetragonal phase and a corresponding decrease of the monoclinic phase content occurs. Increasing the calcium content by two times, from 0.05 to 0.1 leads to a more noticeable but slow change in the phase composition: from 98 to 74 % decrease - for the monoclinic phase and from 2.2 to 22 % increase - for the tetragonal one. Similar changes in phase content take place if the *y* value increases from 0.1 to 0.15. However, within a change of the *y* value from 0.1 to 0.15, the phase composition changes are more significant. Thus, the monoclinic phase content drops from 74 to 13 %, while the tetragonal content increases from 22 to 82 %. The content of the impurity phase increases from 4 to 11 % with a Ca^{2+} ions concentration *y* increasing from 0.05 to 0.2. This phase was previously identified as CaV_2O_6.

As has been pointed out in the Introduction section, we have aimed to find a way to evaluate of the phase content in $La_{1-x-y}Sm_xCa_yVO_{4-\delta}$ using some optical spectroscopy procedures. That is why, the data on the phase content (see Table 1 and Fig. 6) were used by us as references for further spectroscopic analysis. Spectroscopic evaluations have to be based on physical imaginations concerning peculiarities of the Sm^{3+} and Ca^{2+} ions interactions with the neighborhood surrounding the crystal lattice and on the principal features of the electronic processes in the absorption and luminescence centers formed by the dopants. Besides, it should be emphasized that we have to select the characteristics that are

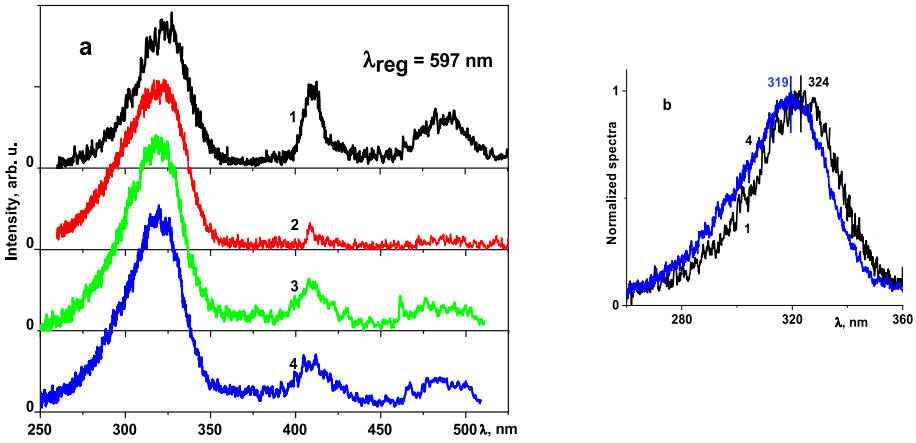

Fig. 8. a): Excitation spectra of the $La_{1-x-y}Sm_xCa_yVO_{4-\delta}$ samples; (x, y) = 0.05 (1), 0.1 (2), 0.15 (3), and 0.2 (4); b): normalized short wavelength band of the 1 and 4 excitation spectra shown in Fig. 8a; λ_{reg} = 597 nm; T = 300 K.

more sensitive to crystal structure transformations.

It is known, that vanadium and lanthanum atoms are coordinated with four and nine oxygen atoms in the monoclinic lattice, respectively, and they are characterized by a C_s local symmetry of the oxygen surrounding [52,57,67]. As for the tetragonal $LaVO_4$ crystal lattice, the La and V cations are located there at higher symmetry positions. The V atoms are also coordinated by four oxygen atoms similar to the case of the monoclinic crystal structure, but here they form perfect VO_4 tetrahedrons of the T_d local symmetry. The La atoms are coordinated by eight oxygen atoms with the D_{2d} local symmetry of the neighboring oxygen surrounding [62].

Both Sm^{3+} and Ca^{2+} dopant ions have to replace mainly La^{3+} ions in the $LaVO_4$ crystal lattice. It should be noted that incorporated Sm^{3+} and Ca^{2+} ions (effective ionic radii are 1.132 and 1.18 Å for the nine-fold coordination, CN = 9, respectively) are smaller than the La^{3+} ions (La^{3+} effective ionic radius is 1.216 Å at CN = 9). So, as a result of the replacement the crystal field strength in the environment of the dopant ions changes which leads to the deformation of the oxygen environment near the dopants and the distortion of the nearest VO_4^{3-} molecular anions.

Besides crystal field perturbations, a necessity to compensate an effective negative charge of the $[Ca^{2+}/La^{3+}]^{-}$ defects is needed in case of the Ca^{2+} substitution in the La^{3+} sites. The compensation can be achieved by the formation of $[V_O]^{2+}$ oxygen vacancies. Thus, one oxygen vacancy can be associated with two Ca^{2+} ions. As a result, both the Sm^{3+} and Ca^{2+} ions incorporation causes deformations of the $LaVO_4$ monoclinic crystal lattice and promote its transformation to the tetragonal one.

Here, the obtained results are undoubtedly consistent with the described features of the placements of samarium and calcium ions in the lattice of the lanthanum orthovanadate. Particularly, as noted above and based on the XRD results of the phase content, evaluations were made on the assumption that dopant ions are located in the La^{3+} ions site positions. This consideration coincides also with optical spectroscopy data about samples under study. There is no doubt, that a set of narrow lines observed in the reflection spectra should be related to the absorption transitions in the *f* shell of the Sm^{3+} ions. There should be $^6H_{5/2} \rightarrow {}^4F_{9/2}$ (360 and 364 nm), $^6H_{5/2} \rightarrow {}^4D_{5/2}$ (374 and 380 nm), $^6H_{5/2} \rightarrow {}^4F_{7/2}$ (404 nm), $^6H_{5/2} \rightarrow {}^6P_{5/2}$ (422 nm), $^6H_{5/2} \rightarrow {}^4G_{9/2}$ (460, and 466 nm), and $^6H_{5/2} \rightarrow {}^4I_{11/2}$ (478 nm) transitions [29–33].

The broad absorption band which is manifested in the reflection spectra and is peaked near 310 nm corresponds to the $O^{2-} \rightarrow V^{5+}$ charge transfer transitions in the VO_4^{3-} vanadate anions [17,68,69]. The bands in the reflection spectra with maxima near 400 and 470 nm, the intensity of which increases in the spectra of the samples doped with calcium should be associated with absorption transitions in defect centers induced by the influence of Ca cations [51,56]. Such bands practically are not observed for the calcium-free $La_{1-x}Sm_xVO_4$ samples (Fig. 3, curve 1). Oxygen vacancies can be responsible for the appearance of these bands [56]. Thus, spectral data on light diffuse reflection show that samarium and calcium ions are included in the lanthanum orthovanadate lattice, and their charge states should be Sm^{3+} and Ca^{2+}, respectively. However, we did not find in these spectra evidence of a direct relationship between their concentration behavior and the phase composition of the studied samples.

It should be emphasized here that variations in the phase composition of the samples could be manifested in a change of their electronic structure because the transformation from the monoclinic to the tetragonal crystal structure is accompanied by a structural change in the $LaVO_4$ lattice. Therefore, we analyzed the effect of Sm^{3+} and Ca^{2+} doping on the band gap of the studied compounds using the data of the diffuse reflectance spectra.

The analysis was made using a well-known Kubelka-Munk transformation (Fig. S2) [70,71]. Evaluated with an inaccuracy of ±0.01 eV the band gap values are 3.85 eV for the samples without calcium, $La_{0.9}Sm_{0.1}VO_4$, as well as 3.82, 3.75, and 3.78 eV for the samples with (x, y) = 0.05, 0.10, and 0.15, respectively. The E_g value of the sample with (x, y) = 0.2 was estimated as 3.62 eV. We suppose this value is incorrect as a result of the significant superposition of the fundamental absorption edge with bands of defects absorption when the dopant concentration is 0.2 (Fig. 3, curve 5). It should be noted, that these values are in accordance with previous estimations, 3.5 eV (354 nm), of the band gap for $LaVO_4$ [72].

Summarizing the made evaluations of the band gap, we can state that the obtained change of the E_g value with (x, y) concentrations can be regarded in correlation with the crystal phase content behavior. At the same time, we have to emphasize that the E_g value changes are only near 1.1 %. We suppose that these E_g changes are too small to be recommended for discussion of a possible correlation of the E_g value with the content of the structural phases in the studied compounds.

We suppose that the characteristics of the PL and the PL excitation spectra have to be more suitable for phase content monitoring. This opinion originates from the specifics of the VO_4^{3-} molecular groups and Sm^{3+} ions energy levels behavior under the transformation of the lanthanum orthovanadate lattice from the monoclinic to the tetragonal crystal structure.

As Fig. 5 shows, an excitation of the Sm^{3+} ions PL takes place, particularly in the wide short-wavelength band (250–350 nm) which corresponds to a similar band in the diffuse reflectance spectra (Fig. 4). These excitation bands are caused by absorption transitions in the VO_4^{3-} molecular groups [73,74]. It is known, that the site symmetry of the VO_4^{3-} groups both in monoclinic *m*-$LaVO_4$ and tetragonal t-$LaVO_4$ crystal lattices is lower than a symmetry of free VO_4^{3-} molecular anions: C_1, D_{2d}, and T_d, respectively, for the noted cases. The crystal field strength in the VO_4^{3-} sites is also different for the m- and t-$LaVO_4$ phases. As a result, the transformation of the lattice from the monoclinic to the tetragonal one can be accompanied by changes in the absorption transition intensities as well as with changes in the 250–350 nm band profile. Fig. 5b illustrates how the mentioned changes in crystal structure are reflected in the shape and peak position of this excitation band.

The absorbed energy from the excited states of the VO_4^{3-} group can be dissipated by radiation way causing wide bands of the own orthovanadate PL in the range 425–750 nm (Fig. 4). It is obvious that monitoring the intrinsic PL band's behavior depending on the phase composition of vanadate has no prospects. These PL bands are too sensitive to the impact of defects and dopants, and in addition, their intensity is strongly suppressed at room temperature (Fig. 4).

Besides, excitation energy can be transferred via a non-radiative way to the luminescent Sm^{3+} ions which can emit delivered energy in a set of relatively narrow lines which result from the $^4G_{5/2} \rightarrow {}^6H_{5/2}$, $^6H_{7/2}$, $^6H_{9/2}$, and $^6H_{11/2}$ radiation transitions in the inner *f* - *f* shell of the Sm^{3+} ions (Figs. 4 and 7) [29–33,75–77]. The groups of lines marked by us in the Section "Results" as I, II, II, and IV correspond with noted types of transitions, respectively. If incident light photons are from the 3.64–2.38 eV (~340–520 nm) range, then Sm^{3+} ions can be excited directly via the intrinsic absorption transitions $^6H_{5/2} \rightarrow {}^4F_{9/2}$, $^4D_{5/2}$, $^4F_{7/2}$, $^6P_{5/2}$, $^4G_{9/2}$, and $^4I_{11/2}$ (Figs. 5 and 8).

The noted PL excitation mechanisms of the Sm^{3+} ions must respond to changes in the structure of the crystal lattice under transformation from one phase to another. Indeed, as it is known, the probability of an excitation energy transfer between molecular groups $VO_4^{3-} \rightarrow VO_4^{3-} \ldots \rightarrow VO_4^{3-}$ and its transfer to RE ions, $VO_4^{3-} \rightarrow RE^{3+}$, is significantly higher for tetragonal vanadates than for monoclinic ones [36,53,70,71]. Therefore, the *m*-$LaVO_4$ → t-$LaVO_4$ transformation should lead to an increase of the wide excitation band (250–350 nm) intensity, that we have just observed (Figs. 5 and 8). At the same time, the intensity of the direct excitation of the Sm^{3+} ions PL (excitation spectrum in 440–520 nm range) located in a higher symmetrical environment in the tetragonal crystal structure compared to the monoclinic one should be lower than in the case of the *m*-$LaVO_4$ phase. A combined effect of these two factors leads to the decrease of the $R_{exc} = I_{long}/I_{short}$ value by ~4.6 and 2.4 times (e.g., at 597 nm registration) when the tetragonal phase

content increases from zero to 2.3 %, and from 2.3 to 84 %, respectively (Fig. 9a, Table S2).

For comparison, we have analyzed the concentration behavior of the relative intensity of the excitation bands belonging only to the long-wavelength part of the excitation spectra: the 385–440 and 440–520 nm bands: $R_{exc}^* = I_{(440-520)}/I_{(385-440)}$. This analysis is also useful as these bands are a result of electronic transitions of different types. These are $^6H_{5/2} \rightarrow {}^4F_{7/2}$, $^6P_{5/2}$ transitions for the first range, and $^6H_{5/2} \rightarrow {}^4G_{9/2}$, $^4I_{11/2}$ transitions for the second range. The calculated R_{exc}^* values are shown in Fig. 9b. The Figure shows that the change of the crystal field under the transformation of the samples from the monoclinic to the tetragonal crystal structure affects with a different rate on the intensity of the above-noted transitions in absorption, that allows, in principle, monitoring the phase composition.

The obtained results reveal a certain relationship between the behavior of the ratio of the intensity of the bands in the excitation spectra and the quantitative content of the phases in the $La_{1-x-y}Sm_xCa_yVO_{4-\delta}$ compound. However, it is appropriate to use these data for estimation of the phases content only if the tetragonal phase content is below 25 % (Fig. 9a and b).

If we continue the discussion about the luminescent monitoring of the phase composition in lanthanum orthovanadates, it should be noted that the observed changes in the luminescent characteristics of Sm^{3+} ions, in principle, can be the result of not only lattice transformation. It should also be taken into account that Ca^{2+} dopant ions can form complex luminescence centers containing Sm^{3+} ions and neighboring oxygen vacancies. Thus, the luminescence of such complex centers could influence the concentration behavior of the Sm^{3+} ions luminescence. However, as we can conclude from the analysis of the high resolution of the PL (Fig. 4) and PL excitation spectra (Fig. 5) a direct influence of the Ca^{2+} ions on energy levels and electronic transitions in Sm^{3+} ions is negligible. Indeed, there were no noticeable changes in the PL line's peak positions. Moreover, a manifestation of new complex luminescence centers in the samples that contain calcium ions should be out of consideration as the intensity of additive PL lines, which appear with the incorporation of Ca^{2+} ions and which could be related to such centers, is also negligible. (These lines are marked by stars in Fig. 4b and in Table S1).

Therefore, we have a strong reason to assume that the concentration behavior of the luminescence characteristics, described in the section "Results" is related just to phase transformations in the compound under study. The following analysis to some extent confirms the view above.

As already mentioned above, the transition from a monoclinic to a tetragonal phase is accompanied by a crystal lattice symmetry increase while the crystal field strength decreases at the Sm^{3+} sites. As a result, the Stark splitting of the ^6H_J multiplets of the ground electronic state of the Sm^{3+} ions should be smaller for the case of a tetragonal phase compared to a monoclinic one. Therefore, if the increase of the t-$LaVO_4$ phase content occurs, the contribution of the Sm^{3+} ions in the *m*-$LaVO_4$ phase to the linear emission spectra should be decreased, which is reflected by the decrease in the spectral contribution of the set of lines marked by pointing down arrows in Fig. 8. Since the range of the PL line's location for the *m*-$LaVO_4$ is wider than for the t-$LaVO_4$, the increase of the t-$LaVO_4$ content is accompanied by a decrease of half-widths of the group's II and III envelopes and by a decrease in the Δ distance between the main peaks in group I (Table S2). The similarity of the behavior of the noted above characteristics indicates the identity of the mechanism that causes the changes and confirms the validity of the approach we used. However, from a practical point of view, the expediency of such an approach used for the phase content estimation is questionable due to the low accuracy of determining both the distance between the peaks in group I and the half-width of the PL groups II and III.

The data from Table 1 show that the sample with the lowest dopant

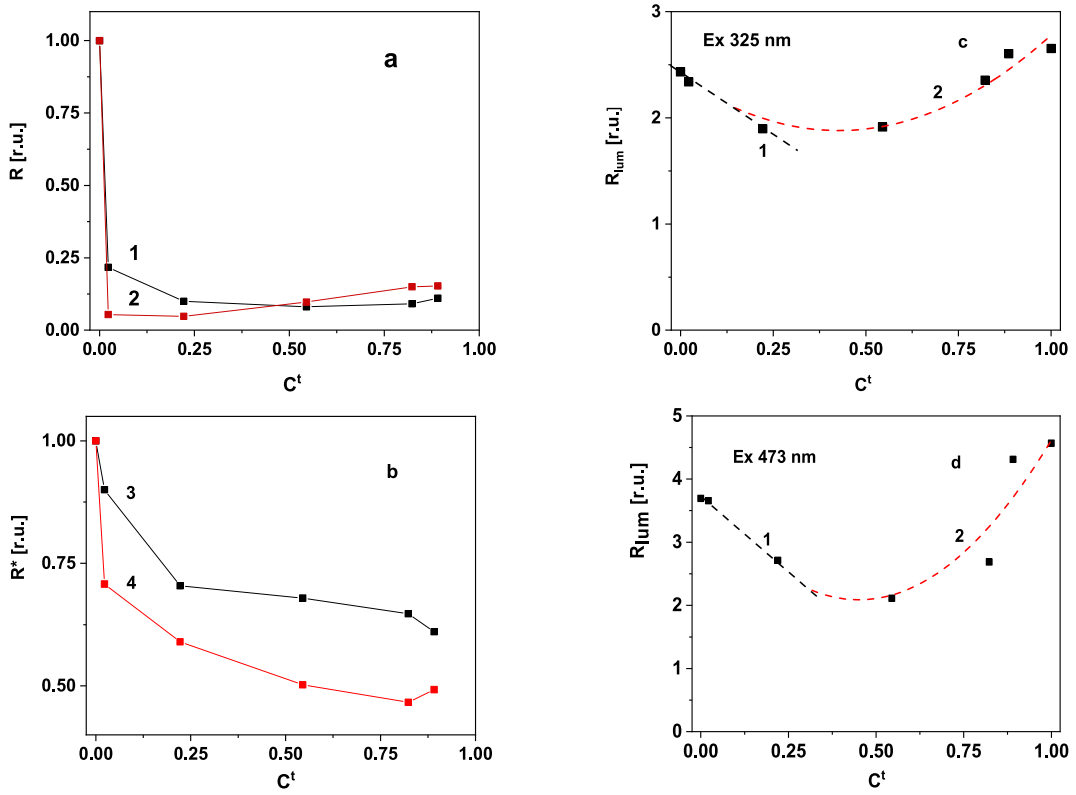

Fig. 9. The dependences of the $R_{exc} = I_{long}/I_{short}$ (a) and $R_{exc}^* = I(440–520)/I(385–440)$ (b) in the excitation spectra measured at λ_{reg} = 597 (1, 3) and 645 nm (2, 4); the dependences of the intensity asymmetric ratios in the luminescence spectra $R_{lum} = I_{(III)}/I_{(I)}$; λ_{ex} = 325 (c), and 473 nm (d) on the tetragonal phases content C^t in the $La_{1-x-y}Sm_xCa_yVO_{4-\delta}$ samples. The symbols mark experimental data; dashed black lines (1) are linear approximations, and dashed red curves are polynomial approximation of the experimental data.

concentrations, (x, y) = 0.05, consists of ~98 % *m*-$LaVO_4$ phase, and therefore the PL spectra of the sample (Fig. 7, curves 1) mainly represent the emission of this phase: *m*-$LaVO_4$. Similarly, the sample with the highest, (x, y) = 0.2), dopant concentrations consist of ~89 % t-$LaVO_4$ phase, and therefore the PL spectrum in Fig. 7, curves 4) to some extent can be taken as representatives of the tetragonal phase emission. Taking into account the noted consideration we tried to present the PL spectra of the samples with intermediate concentrations of dopants by combinations of contributions of the indicated reference spectra (Fig. S3). One can find that spectra of the $La_{0.8}Sm_{0.1}Ca_{0.1}VO_{4-\delta}$ and $La_{0.7}Sm_{0.15}Ca_{0.15}VO_{4-\delta}$ samples with intermediate concentrations of dopants can be represented by the sums of both types of emission with high accuracy. The contributions of the m- and t-phases to the total emission have to be chosen for those cases as (96, and 4 %) for the first, and (32, and 68 %) for the second case, respectively. The used values of contributions substantially differ from the ratio of crystal phases content obtained from the XRD analysis (74 and 22 %) for the first case ($La_{0.8}Sm_{0.1}Ca_{0.1}VO_{4-\delta}$), and (13 and 82 %) for the latter case of the samples ($La_{0.7}Sm_{0.15}Ca_{0.15}VO_{4-\delta}$). Therefore, we suppose that some additional factors must be taken into consideration.

Now, we will consider the possibility of evaluating the changes in phase composition using the ratio of the ($I_{(I)}$) and III ($I_{(III)}$) intensity in each of the emission spectra in Fig. 7. The physical basis for such analysis is that these groups are caused by electronic transitions of various types. The $^4G_{5/2} \rightarrow {}^6H_{5/2}$ transition (group I, peaked at 561 nm) is a magnetic dipole (MD) allowed one, thus its intensity is of low sensitivity to the local symmetry of the neighbour environment. The $^4G_{5/2} \rightarrow {}^6H_{7/2}$ transition (group II, peaked at 597 nm for low and near 601 nm for the high concentration of dopants) is a mixed magnetic-electric dipole transition (MD + ED) according to the selection rules. The $^4G_{5/2} \rightarrow {}^6H_{9/2}$ (group III, peaked at 645 nm) is an electric dipole (ED) allowed transition. The last transition is sensitive to the crystal field and it is known as a hypersensitive transition. In the case of the inverse local symmetry of the Sm^{3+} ions, the intensity of the $^4G_{5/2} \rightarrow {}^6H_{9/2}$ transition should be higher than the intensity of the $^4G_{5/2} \rightarrow {}^6H_{5/2}$ and $^4G_{5/2} \rightarrow {}^6H_{7/2}$ transitions, while in the case of the non-inverse local symmetry, the intensity of the $^4G_{5/2} \rightarrow {}^6H_{9/2}$ transition should be lower than the intensity of the $^4G_{5/2} \rightarrow {}^6H_{5/2}$ and $^4G_{5/2} \rightarrow {}^6H_{7/2}$ transitions [22,29–33].

The measured PL spectra have revealed an absence of the inverse center for the Sm^{3+} ions in the compositions under study (Figs. 4 and 7). As a local symmetry of the Sm^{3+} ions is determined mainly by their belonging to *m*-$LaVO_4$ or t-$LaVO_4$ crystal phases, then the ratios $R_{lum} = I_{(III)}/I_{(I)}$ (asymmetry ratio) of the intensities of radiation transitions can be used for finding a possible correlation with phase composition behavior. Indeed, the dependencies shown in Fig. 9 (dash red approximating curves) show smooth changes in the R_{lum} values depending on the phase composition of the samples. (Parameters of the approximating curves can be seen in Supplementary, Part III.) So, we have to state that the transformation of the monoclinic phase to the tetragonal one occurs without any jumps (see also Fig. 6a). Since the sample with y = 0 consists only of the monoclinic phase ($C^t = 0$), the value of $R_{lum}(C^t = 0)$ corresponds to the luminescence characteristic of the monoclinic phase, $R_{lum}(C^t = 0) = R^m$. According to the approximation results, $R^m = 2.44$ and 3.72, for excitation with $\lambda_{ex} = 325$ and 473 nm, respectively. We see also that the decrease of the R_{lum} in the range C^t value 0–0.3 correlates with the monoclinic phase amount decreasing. The R_{lum} decrease is caused by an increase in the content of the tetragonal phase, for which, as was mentioned above, the value of the asymmetric ratio, R^t, should be lower than R^m, $R^t < R^m$.

With a further change in the phase content ((x, y) are from the range 0.11–0.14; C^m and C^t lie in the range 0.4–0.6) the R_{lum} value practically does not change. Assuming in the zero approximation, that the contribution of each phase to R_{lum} is proportional to the amount of the phase and taking at $C^t = 0.5$ that $R_{lum} = 1.88$, the R^t value was evaluated as 1.32. The R^t for the case with $\lambda_{ex} = 473$ nm was estimated as 1.46.

Thus, it can be supposed that the concentration behavior of the R_{lum} value in the range of the concentrations of dopants (x, y) from zero to 0.11 ($C^t = 0.3$) can be used for evaluation of both the phases content and their asymmetric ratio luminescence characteristics in compounds under study.

Finally, we found that with a further increase of the content of the dopants (with an increase of the tetragonal phase content), the R_{lum} value also increases (Fig. 9c and d). It should be emphasized, that the noted increase of the R_{lum} value takes place at a rather low PL intensity and the changes are within the limits of 4 % (Fig. 6, curve 4). However, this R_{lum} value increase correlates with the increase in PL intensity. Therefore, we found it necessary to analyze more detailed its possible origins. Thus, analyzing and comparing data shown in Fig. 9c and d we see that the R_{lum} dependences can be determined at least by two factors. The first one is determined by various types of luminescence excitation, as $\lambda_{ex} = 325$ nm represents excitation via host, VO_4^{3-} molecular groups, while the 473 nm excitation occurs via absorption transitions directly within the *f* - shell of the Sm^{3+} ions. The second one, undoubtedly, is an influence of the phase's content.

When considering the last factor, we concluded that there is no reason to consider the studied samples as a simple mixture of two phases, especially at a high content of the tetragonal phase ($C^t > 0.5$). If C^t increases from ~0.6 to 1.0, the R_{lum} value increases. Therefore, the case $R^t > R^m$ should be fulfilled there. However, it is obvious that both the R^t and R^m values should not depend on the amount of the starting phases. Therefore, a change in these values has to be considered as a change in the phases themselves. Thus, the described behavior should be considered as a contribution of some third phase which content increases with C^t increasing. This phase exhibits an appropriate asymmetric ratio and the following relation must hold for its value $R^* > R^m > R^t$. Taking into account that the monoclinic phase at $C^t = 0.9$ is absent in the composition of the samples and assuming in the zero approximation, that the contribution of the mentioned phase is 10 %, the R* values can be estimated as equal to 13 and 25 for the cases with excitation at 325 and 473 nm, respectively. Therefore, the ratio $R^* > R^m > R^t$ is fulfilled.

It should be mentioned here that the results of the XRD analysis also revealed the presence of a third component in the composition of the samples. The obtained data showed that the CaV_2O_6 compound can be the additive phase, with a volume reaching 11 % at a high content of dopants. At the same time, a low probability of the La and Sm ions entering this phase was established from the data of the XRD analysis. This conclusion was also confirmed by EDS analysis data (see Suppl. materials, part IV). So, if the Sm^{3+} ions were not included in this phase, it would be very difficult to explain its possible effect on the luminescence spectral characteristics discussed above.

In our opinion, the intermediate layers between the particles of different crystal structures can be regarded as the additive phase active in luminescence. This layered phase can be formed at synthesis of the samples. The thickness of such layers can be quite small, and their structures, due to the mutual diffusion of constituents of monoclinic and tetragonal phases, can be uncertain. As a result, this component is not determined by the XRD method, even, as in our case, with the high sensitivity of the XRD used. However, as the concentration of tetragonal phase particles increases, the total amount of the intermediate phase C* increases, and therefore its influence on the macro-characteristics of the material can also increases. Applied luminescence procedures, due to the ultra-sensitivity of electronic transitions with absorption and emission of light to the symmetry of the Sm^{3+} ions, allowed to register manifestations of the additional component of the phase composition with an increase of the tetragonal phase nanoparticles content. It should be assumed that the local symmetry of the Sm^{3+} ions can be low in the intermediate layers of a disordered structure of the crystal lattice, and the crystal field in these layers can be strong. This fact can ensure the above-mentioned ratio $R^* > R^m > R^t$, and therefore it satisfies the increase in R_{lum} with C^t increasing.

Another factor that ensures a significant increase of the R_{lum} at a high

C^t value at a relatively low volume of the intermediate layers is an intensification of excitation energy transfer through the tetragonal phase particles when their amount increases. Similar behaviors of the R_{exc} which characterize excitation spectra and the R_{lum} value characterizing emission spectra in the range of $C^t > 0.22$ confirm an important role of the excitation energy transfer (Fig. 9).

We suppose that the above-noted data and its description confirmed the possibility of using an experimentally measured "asymmetric" ratio R_{lum} in luminescence spectra of Sm^{3+} ions for monitoring the monoclinic and tetragonal phases content over all possible ranges of their changing.

5. Conclusions

The set of the $La_{1-x-y}Sm_xCa_yVO_{4-\delta}$ crystalline nanoparticles ($x = y$; (x, y) = 0.05–0.2) were synthesized for the first time. The citrate-nitrate sol-gel method was successfully used for the synthesis.

The synthesized samples are characterized mainly by two-phase composition. They contain nanoparticles of monazite and zircon structures, and monoclinic and tetragonal crystal lattices, respectively. The increase of the Ca^{2+} ions amount leads to an increase of the tetragonal phase content C^t from zero ($y = 0$) to 2.3 % ($y = 0.05$) and 88.6 % ($y = 0.2$). Simultaneously, the monoclinic phase content C^m decreases from 100 % ($y = 0$) to 73.7 % ($y = 0.05$), and to zero percent ($y = 0.2$).

Optical (diffuse reflectance and luminescence) characteristics of the samples have been analyzed in connection with the crystal phase content.

- It was found that the band gap (E_g) values reflect to some degree the phase composition of the samples, but E_g changes are too small to be observed for a reliable correlation of their behavior with the phase content behavior.
- The photoluminescence spectra of the $La_{1-x-y}Sm_xCa_yVO_{4-\delta}$ contain four groups of lines (I – IV) resulting from radiation transitions $^4G_{5/2} \rightarrow {}^6H_{5/2}$, $^6H_{7/2}$, $^6H_{9/2}$, and $^6H_{11/2}$, respectively, in the inner *f* - *f* shell of the Sm^{3+} ions. It was found that this luminescence is a superposition of emission of the Sm^{3+} ions located in the monoclinic and tetragonal phases. As the site symmetry and crystal field stretches are different for the Sm^{3+} ions arranged in crystal lattices of the noted phases, luminescence characteristics of the Sm^{3+} ion's are different for these two phases. That is why, the concentration behavior of the Sm^{3+} ions luminescence characteristics is related to changing the $La_{1-x-y}Sm_xCa_yVO_{4-\delta}$ phase composition.
- The measured dependences of the total intensity for both luminescence emission and excitation spectra, can be used, in principle, for the phase content monitoring, but the differential method which uses the $R_{lum} = I_{(III)}/I_{(I)}$ asymmetry ratio is more accurate for the noted monitoring.
- Formation of the luminescence active additional phase at the highest dopant concentration, which is the result of the monoclinic and tetragonal phases mutual diffusion, was assumed from the R_{lum} behavior. The assumption about the formation of such an additional phase and its role in phase transformation and luminescence processes has to be confirmed by future studies.

The complex procedure of evaluation of the data about the correlation of the structural and optical spectroscopic characteristics can be used in the further engineering of the phosphors based on both lanthanum orthovanadates and other multiphase oxide compounds containing the Sm^{3+} ions.

CRediT authorship contribution statement

S.G. Nedilko: Writing – review & editing, Writing – original draft, Supervision, Resources, Methodology, Investigation, Data curation, Conceptualization. **O. Chukova:** Writing – original draft, Investigation, Data curation, Conceptualization. **A. Dorofieieva:** Validation, Investigation, Data curation. **S.A. Nedilko:** Validation, Supervision, Formal analysis. **V. Shcherbatskyi:** Investigation, Data curation. **T. Voitenko:** Methodology, Investigation. **M. Etter:** Investigation, Data curation. **H.S. Rahimi Mosafer:** Methodology, Investigation, Data curation. **W. Paszkowicz:** Writing – review & editing, Supervision, Formal analysis, Data curation. **Y. Zhydachevskyy:** Investigation, Formal analysis, Data curation. **A. Suchocki:** Writing – review & editing, Investigation, Formal analysis, Data curation.

Compliance with ethical standards

This paper contains no research involving human participants and/or animals.

Declaration of competing interest

The authors declare that they have no known competing financial interests or personal relationships that could have appeared to influence the work reported in this paper.

Acknowledgements

This work received funding from the Ministry of Education and Science of Ukraine and partially from the Polish National Agency for Academic Exchange (Bilateral Grant Program).

Serhii Nedilko thanks the Polish Academy of Sciences for the possibility of research stay and spectroscopy measurements at the Institute of Physics PAS, Warsaw, Poland. Oksana Chukova acknowledges funding from the MSCA4Ukraine project, which is funded by the European Union (Grant agreement 101101923).

The work also was supported by the Horizon Europe research and innovation program under grant agreement No 654360 having benefited from the access provided by the Institute of Electronic Structure & Laser (IESL) of Foundation for Research & Technology Hellas (FORTH) in Heraklion, Crete, Greece; Division of Microscopy of Universitat Autonoma de Barcelona, Spain; Deutsches Elektronen-Synchrotron (DESY) Hamburg, Germany within the framework of the NFFA-Europe Transnational Access Activity.

Appendix A. Supplementary data

Supplementary data to this article can be found online at https://doi.org/10.1016/j.omx.2024.100390.

Data availability

Data will be made available on request.

References

[1] Y. Zhuo, J. Brgoch, Opportunities for next-generation luminescent materials through artificial intelligence, J. Phys. Chem. Lett. 12 (2021) 764–772, https://doi.org/10.1021/acs.jpclett.0c03203.
[2] A.K. Soni, B.P. Singh, Luminescent materials in lighting, display, solar cell, sensing, and biomedical applications, in: Luminescence - OLED Technology and Applications. London, United Kingdom, 2019.
[3] R.S. Boyko, O.V. Chukova, O.V. Gomenyuk, P.G. Nagornyi, S.G. Nedilko, Origin of red luminescence of sodium titanium phosphate crystals, Phys. Status Solidi C 2 (2005) 712–715, https://doi.org/10.1002/pssc.200460272.
[4] R. Lisiecki, J. Komar, B. Macalik, M. Głowacki, M. Berkowski, W. Ryba-Romanowski, Exploring the impact of structure-sensitivity factors on thermographic properties of Dy^{3+} - doped oxide crystals, Materials 14 (19) (2021) 2370, https://doi.org/10.3390/ma14092370.
[5] X. Huang, S. Han, W. Huang, X. Liu, Enhancing solar cell efficiency: the search for luminescent materials as spectral converters, Chem. Soc. Rev. 42 (2013) 173–201, https://doi.org/10.1039/c2cs35288e.
[6] C.C. Lin, W. Chen, R.S. Liu, Phosphors for white LEDs, in: R. Karlicek, C.C. Sun, G. Zissis, R. Ma (Eds.), Handbook of Advanced Lighting Technology, Springer Cham, Cham, Switzerland, 2017, pp. 182–222.
[7] P.K. Tawalare, Luminescent inorganic mixed borate phosphors materials for lighting, Luminescence 37 (2022) 1226–1245, https://doi.org/10.1002/bio.4301.

[8] J. Li, J. Yan, D. Wen, Wasim U. Khan, J. Shi, M. Wu, Q. Su, P.A. Tanner, Advanced red phosphors for white light-emitting diodes, J. Mater. Chem. C 4 (2016) 8611–8623, https://doi.org/10.1039/c6tc02695h.

[9] B.M. Van der Ende, L. Aarts, A. Meijerink, Lanthanide ions as spectral converters for solar cells, Phys. Chem. Chem. Phys. 11 (2009) 11081–11095, https://doi.org/10.1039/b913877c.

[10] V. Chornii, O. Chukova, S.G. Nedilko, S.A. Nedilko, T. Voitenko, Enhancement of emission intensity of $LaVO_4:RE^{3+}$ luminescent solar light absorbers, Phys. Status Solidi C 13 (2016) 40–46, https://doi.org/10.1002/pssc.201510116.

[11] Z. Yang, G. Liu, Y. Zhao, Y. Zhou, J. Qiao, M.S. Molokeev, H.C. Swart, Z. Xia, Competitive site occupation toward improved quantum efficiency of $SrLaScO_4$:Eu red phosphors for warm white LEDs, Adv. Opt. Mater. 10 (2022) 2102373, https://doi.org/10.1002/adom.202102373.

[12] L. Li, M. Dou, Y. Yan, Y. Li, F. Ling, S. Jiang, G. Xiang, J. Liu, X. Zhou, Insight into energy transfer, colour tuning, and white emission in Tm^{3+} and Dy^{3+} codoped $Ca_8ZnLa(PO_4)_7$ phosphors, Opt. Mater. 102 (2020) 109808, https://doi.org/10.1016/j.optmat.2020.109808.

[13] C.H. Huang, T.M. Chen, A novel single-composition trichromatic white-light $Ca_3Y(GaO)_3(BO_3)_4:Ce^{3+}$, Mn^{2+}, Tb^{3+} phosphor for UV-light emitting diodes, J. Phys. Chem. C 115 (2011) 2349–2355, https://doi.org/10.1021/jp107856d.

[14] S. Schmiechen, H. Schneider, P. Wagatha, C. Hecht, P.J. Schmidt, W. Schnick, Toward new phosphors for application in illumination-grade white pc-LEDs: the nitridomagnesosilicates $Ca[Mg_3SiN_4]:Ce^{3+}$, $Sr[Mg_3SiN_4]:Eu^{2+}$, and $Eu[Mg_3SiN_4]$, Chem. Mater. 26 (2014) 2712–2719, https://doi.org/10.1021/cm500610v.

[15] D.J. Jovanović, 6 - lanthanide-doped orthovanadate phosphors: syntheses, structures, and photoluminescence properties, in: S.J. Dhoble, V.B. Pawade, H. C. Swart, V. Chopra (Eds.), Woodhead Publishing Series in Electronic and Optical Materials, Spectroscopy of Lanthanide Doped Oxide Materials, Woodhead Publishing, Cambridge, United Kingdom, 2020, pp. 235–291.

[16] M. Michalska, J.B. Jasiński, J. Pavlovsky, P. Żurek-Siworska, A. Sikora, P. Gołębiewski, A. Szysiak, V. Matejka, J. Seidlerova, Solid state-synthesized lanthanum orthovanadate ($LaVO_4$) Co-doped with Eu as efficient photoluminescent material, J. Lumin. 233 (2021) 117934, https://doi.org/10.1016/j.jlumin.2021.117934.

[17] O. Chukova, S.G. Nedilko, S.A. Nedilko, T. Voitenko, O. Gomenyuk, V. Sheludko, Study of temperature behavior of luminescence emission of $LaVO_4$ and $La_{1-x}Eu_xVO_4$ powders, Solid State Phenom. 230 (2015) 153–159. https://doi.org/10.4028/www.scientific.net/ssp.230.153.

[18] M.K. Mahata, S.P. Tiwari, S. Mukherjee, K. Kumar, V.K. Rai, $YVO_4:Er^{3+}/Yb^{3+}$ phosphor for multifunctional applications, J. Opt. Soc. Am. B 31 (2014) 1814–1821, https://doi.org/10.1364/JOSAB.31.001814.

[19] H.-Y. Lin, W.-F. Chang, S.-Y. Chu, Luminescence of $(Ca,Sr)_3(VO_4)_2:Pr^{3+}$, Eu^{3+} phosphor for use in CuPc-based solar cells and white light-emitting diodes, J. Lumin. 133 (2013) 194–199, https://doi.org/10.1016/j.jlumin.2011.12.034.

[20] T. Nakajima, M. Isobe, T. Tsuchiya, Y. Ueda, T. Manabe, Correlation between luminescence quantum efficiency and structural properties of vanadate phosphors with chained, dimerized, and isolated VO_4 tetrahedra, J. Phys. Chem. C 114 (2010) 5160–5167, https://doi.org/10.1021/jp910884c.

[21] G. Panayiotakis, D. Cavouras, I. Kandarakis, C. Nomicos, A study of X-ray luminescence and spectral compatibility of europium-activated yttrium-vanadate (YVO_4:Eu) screens for medical imaging applications, Appl. Phys. A 62 (1996) 483–486, https://doi.org/10.1007/BF01567121.

[22] F.C. Palilla, A.K. Levine, M. Rinkevics, Rare earth activated phosphors based on yttrium orthovanadate and related compounds, J. Electrochem. Soc. 112 (1965) 776–779, https://doi.org/10.1149/1.2423693.

[23] T. Higuchi, Y. Hotta, Y. Hikita, S. Maruyama, Y. Hayamizu, H. Akiyama, H. Wadati, D.G. Hawthorn, T.Z. Regier, R.I.R. Blyth, G.A. Sawatzky, H.Y. Hwang, $LaVO_4$:Eu Phosphor films with enhanced Eu solubility, Appl. Phys. Lett. 98 (2011) 071902, https://doi.org/10.1063/1.3554749.

[24] A. Shyichuk, R.T. Moura Jr., A.N. Carneiro Neto, M. Runowski, M.S. Zarad, A. Szczeszak, S. Lis, O.L. Malt, Effects of dopant addition on lattice and luminescence intensity parameters of Eu(III)-Doped lanthanum orthovanadate, J. Phys. Chem. C 120 (2016) 28497–28508, https://doi.org/10.1021/acs.jpcc.6b10778.

[25] W. Paszkowicz, J. López-Solano, P. Piszora, B. Bojanowski, A. Mujica, A. Muñoz, Y. Cerenius, S. Carlson, H. Dąbkowska, Equation of state and electronic properties of $EuVO_4$: a high-pressure experimental and computational study, J. Alloys Compd. 648 (2015) 1005–1016, https://doi.org/10.1016/j.jallcom.2015.06.211.

[26] K. Li, R. Van Deun, Eu^{3+}/Sm^{3+}-doped $Na_2BiMg_2(VO_4)_3$ from substitution of Ca^{2+} by Na^+ and Bi^{3+} in $Ca_2NaMg_2(VO_4)_3$: color-tunable luminescence via efficient energy transfer from VO_4^{3-} to Eu^{3+}/Sm^{3+} ions, Dyes Pigments 155 (2018) 258–264, https://doi.org/10.1016/j.dyepig.2018.03.050.

[27] E. Bandiello, D. Errandonea, F. Piccinelli, M. Bettinelli, D. Díaz-Anichtchenko, C. Popescu, Characterization of flux-grown $Sm_xNd_{1-x}VO_4$ compounds and high-pressure behavior for x = 0.5, J. Phys. Chem. C 123 (2019) 30732–30745, https://doi.org/10.1021/acs.jpcc.9b09473.

[28] N. Bednarska-Adam, M. Kuwik, T. Goryczka, W. Pisarski, J. Pisarska, Red-emitting olivine-type ceramic luminophores Li_2MGeO_4 (M = Zn, Mg) doped with Sm^{3+}, Opt. Mater. X. 22 (2024) 100311 https://doi.org/10.1016/j.omx.2024.100311.

[29] F. He, P. Yang, D. Wang, N. Niu, S. Gai, X. Li, M. Zhang, Hydrothermal synthesis, dimension evolution and luminescence properties of tetragonal $LaVO_4$:Ln (Ln = Eu^{3+}, Dy^{3+}, Sm^{3+}) nanocrystals, Dalton Trans. 40 (2011) 11023–11030, https://doi.org/10.1039/c1dt11157d.

[30] M. Yu, J. Lin, Z. Wang, J. Fu, S. Wang, H.J. Zhang, Y.C. Han, Fabrication, patterning, and optical properties of nanocrystalline YVO_4: a (A = Eu^{3+}, Dy^{3+}, Sm^{3+}, Er^{3+}) phosphor films via sol–gel soft lithography, Chem. Mater. 14 (2002) 2224–2231, https://doi.org/10.1021/cm011663y.

[31] W.J. Park, M.K. Jung, T. Masaki, S.J. Im, D.H. Yoon, Characterization of $YVO_4:Eu^{3+}$, Sm^{3+} red phosphor quick synthesized by microwave rapid heating method, Mater. Sci. Eng. B 146 (2008) 95–98, https://doi.org/10.1016/j.mseb.2007.07.090.

[32] O.V. Chukova, S.A. Nedilko, S.G. Nedilko, A. Papadopoulos, A.A. Slepets, E. I. Stratakis, T.A. Voitenko, Structure and spectroscopy characterization of $La_{1-x}Sm_xVO_4$ luminescent nanoparticles synthesized co-precipitation and sol-gel methods, Opt. Mater. 95 (2019) 109248, https://doi.org/10.1016/j.optmat.2019.109248.

[33] M. Sobszyk, D. Szymański, A study of optical properties of Sm^{3+} ions in α-$Na_3Y(VO_4)_2$ single crystals, J. Lumin. 142 (2013) 96–102, https://doi.org/10.1016/j.optmat.2012.10.043.

[34] V. Tucureanu, A. Matei, A.M. Avram, Synthesis and characterization of YAG:Ce phosphors for white LEDs, Opto−Electron, Rev. E. 23 (2015) 239–251, https://doi.org/10.1515/oere−2015−0038.

[35] J.H. Kang, W.B. Im, D. Chin Lee, J.Y. Kim, D.Y. Jeon, Y.C. Kang, K.Y. Jung, Correlation of photoluminescence of (Y, Ln)$VO_4:Eu^{3+}$ (Ln = Gd and La) phosphors with their crystal structures, Solid State Commun. 133 (2005) 651–656, https://doi.org/10.1016/j.ssc.2005.01.004.

[36] R. Cao, T. Huang, J. Nie, L. Zhang, Y. Chen, L. Li, B. Lan, J. Wang, Energy transfer and tunable-color luminescence properties of a single-phase $CaSrNb_2O_7:Sm^{3+}$, Bi^{3+}, J. Mol. Struct. 1297 (2024) 136962 https://doi.org/10.1016/j.molstruc.2023.136962.

[37] O. Chukova, S. Nedilko, V. Sheludko, Crystallographic features and nature of luminescence centres of the niobate and tantalate compounds with layered perovskite-like structure, Open Mater. Sci. J. 12 (2018) 2–13, https://doi.org/10.2174/1874088X01812010002.

[38] K.V. Terebilenko, V.P. Chornii, V.O. Zozulia, I.O. Guralskyi, S.G. Shova, S. G. Nedilko, M.S. Slobodyanik, Crystal growth, layered structure and luminescence properties of $K_2Eu(PO_4)(WO_4)$, RSC Adv. 12 (2022) 8901–8907, https://doi.org/10.1039/D2RA00932C.

[39] G. Malashkevich, Yu Bokshits, O. Chukova, V. Koukhar, S. Nedilko, G. Shevchenko, Influence of gold nanoparticles on luminescence of Eu^{3+} ions sensitized by structural defects in germanate films, J. Phys. Chem. C 120 (2016) 15369–15377, https://doi.org/10.1021/acs.jpcc.6b02324.

[40] Z. Xu, C. Li, Z. Hou, C. Peng, J. Lin, Morphological control and luminescence properties of lanthanide orthovanadate $LnVO_4$ (Ln = La to Lu) nano-/microcrystals via hydrothermal process, CrystEngComm 13 (2011) 474–482, https://doi.org/10.1039/C0CE00161A.

[41] R. Lisiecki, W. Ryba-Romanowski, E. Cavalli, M. Bettinelli, Optical spectroscopy of Er^{3+} -doped $LaVO_4$ crystal, J. Lumin. 130 (2010) 131–136, https://doi.org/10.1016/j.jlumin.2009.07.037.

[42] F.P. Riello, F. Enrichi, D. Cristofori, A. Benedetti, Synthesis and optical properties of sub-micron sized rare earth-doped zirconia particles, Opt. Mater. 33 (2011) 1745–1752, https://doi.org/10.1016/j.optmat.2011.06.010.

[43] L. Li, H.K. Yang, B.K. Moon, B.C. Choi, J.H. Jeong, K.-W. Jang, H.S. Lee, S.S. Yi, Structure, charge transfer bands and photoluminescence of nanocrystals tetragonal and monoclinic ZrO_2:Eu, J. Nanosci. Nanotechnol. 11 (2011) 350–357, https://doi.org/10.1166/jnn.2011.3217.

[44] V. Chornii, S.G. Nedilko, M. Miroshnichenko, K. Terebilenko, M. Slobodyanik, Influence of fluorination on structure and luminescence of ZrO_2:Eu nanocrystals, Mater. Res. Bull. 90 (2017) 237–243, https://doi.org/10.1016/j.materresbull.2017.02.033.

[45] E. Radha, D. Komaraiah, R. Sayanna, J. Sivakumar, Photoluminescence and photocatalytic activity of rare earth ions doped anatase TiO_2 thin films, J. Lumin. 244 (2022) 118727, https://doi.org/10.1016/j.jlumin.2022.118727.

[46] J.N.L. Lopes, J.C.S. Filho, D.N. Messias, V. Pilla, Nd^{3+}- doped TiO_2 nanocrystals: structural changes, excited-state dynamics, and luminescence defects, J. Lumin. 240 (2021) 118461, https://doi.org/10.1016/j.jlumin.2021.118461.

[47] S. Cho, Properties of Eu-doped YVO_4 thin films grown on glass substrates by radio-frequency magnetron sputtering, Appl. Phys. A 127 (2021) 161, https://doi.org/10.1007/s00339-021-04308-z.

[48] J.E. Muñoz-Santiuste, U.R. Rodríguez-Mendoza, J. González-Platas, V. Lavín, Structural study of the Eu^{3+} environments in fluorozirconate glasses: role of the temperature-induced and the pressure-induced phase transition processes in the development of a rare earth's local structure model, J. Chem. Phys. 130 (2009) 154501, https://doi.org/10.1063/1.3100770.

[49] M. Faucher, P. Caro, Optical study of $LaAlO_3$:Eu at temperatures approaching the rhombohedric → cubic transition, J. Chem. Phys. 63 (1975) 446–454, https://doi.org/10.1063/1.431125.

[50] P.A. Tanner, C. Rudowicz, Eu^{3+} ion luminescence crystal structure determination for lanthanide sesquioxides, Appl. Spectrosc. 47 (1993) 127–128. https://opg.optica.org/as/abstract.cfm?URI=as-47-1-127.

[51] O.V. Chukova, S.G. Nedilko, A.A. Slepets, S.A. Nedilko, T.A. Voitenko, M. Androulidaki, A. Papadopoulos, E.I. Stratakis, Structure, morphology, and spectroscopy studies of $La_{1-x}RE_xVO_4$ nanoparticles synthesized by various methods, in: O. Fesenko, L. Yatsenko (Eds.), Nanocomposites, Nanostructures, and Their Applications, Springer Proceedings in Physics, Springer, Cham, 2019, pp. 211–241.

[52] S.W. Park, H.K. Yang, J.W. Chung, Y. Chen, B.K. Moon, B.C. Cho, J.H. Jeon, J. H. Kim, Photoluminescent properties of $LaVO_4$ Eu^{3+} by structural transformation, Physica B 405 (2010) 4040–4044, https://doi.org/10.1016/j.physb.2010.06.052.

[53] R. van Deun, M. D'hooge, A. Savic, I.V. Driessche, K.V. Hecke, A.M. Kaczmarek, Influence of Y^{3+}, Gd^{3+}, and Lu^{3+} co-doping on the phase and luminescence

properties of monoclinic Eu:$LaVO_4$ particles, Dalton Trans. 44 (2015) 18418–18426, https://doi.org/10.1039/c5dt03147h.
[54] C.K. Rastogi, S.K. Sharma, A. Patel, G. Parthasarathy, R.G.S. Pala, J. Kumar, S. Sivakumar, Dopant induced stabilization of metastable zircon-type tetragonal $LaVO_4$, J. Phys. Chem. C 121 (2017) 16501–16512, https://doi.org/10.1021/acs.jpcc.7b04508.
[55] R. Okram, G. Phaomei, N.R. Singh, Water driven enhanced photoluminescence of Ln (= Dy^{3+}, Sm^{3+}) doped $LaVO_4$ nanoparticles and effect of Ba^{2+} co-doping, Mater. Sci. Eng. B 178 (2013) 409–416, https://doi.org/10.1016/2Fj.mseb.2013.01.007.
[56] O. Chukova, S.A. Nedilko, S.G. Nedilko, T. Voitenko, A. Slepets, M. Androulidaki, A. Papadopoulos, E. Stratakis, W. Paszkowicz, Strong Eu^{3+} luminescence in $La_{1-x-y}Er_{x/2}Eu_{x/2}Ca_yVO_4$ nanocrystals: the result of co-doping optimization, J. Lumin. 242 (2022) 118587, https://doi.org/10.1016/j.jlumin.2021.118587.
[57] C.J. Jia, L.D.S. Zheng, G.Y. Yu, C.P. Shao, Z.L. Chun, H. Yan, Monazite and zircon type $LaVO_4$:Eu nanocrystals – synthesis, luminescent properties, and spectroscopic identification of the Eu^{3+} sites, Eur. J. Inorg. Chem. 18 (2010) 2626–2635, https://doi.org/10.1002/ejic.201000038.
[58] J. Fan, Y. Li, I. Fryc, C. Qian, X. Fan, G. Zhang, Machine-learning assisted prediction of spectral power distribution for full-spectrum white light-emitting diode, IEEE Photon. J. 12 (2020) 8200218, https://doi.org/10.1109/jphot.2019.2962818.
[59] H.M. Rietveld, A profile refinement method for nuclear and magnetic structures, J. Appl. Crystallogr. 2 (1969) 65–71, https://doi.org/10.1107/S0021889869006558.
[60] C.E. Rice, W.R. Robinson, Lanthanum orthovanadate, Acta Crystallogr. Sect. B Struct. Crystallogr. Cryst. Chem. 32 (1976) 2232–2233, https://doi.org/10.1107/S0567740876007450.
[61] D.F. Mullica, E.L. Sappenfield, M.M. Abraham, B.C. Chakoumakos, L.A. Boatner, Structural investigations of several LnVO4 compounds, Inorg. Chim. Acta. 248 (1996) 85–88, https://doi.org/10.1016/0020-1693(95)04971-1.
[62] Y. Oka, T. Yao, N. Yamamoto, Hydrothermal synthesis of lanthanum vanadates: synthesis and crystal structures of zircon-type $LaVO_4$ and a new compound LaV_3O_9, J. Solid State Chem. 152 (2000) 486–491, https://doi.org/10.1006/jssc.2000.8717.
[63] J.C. Bouloux, G. Perez, Jean Galy, Bulletin de la Societe, Francaise de Mineralogie et de Cristallographie, vol. 95, 1972, pp. 130–133, https://doi.org/10.3406/bulmi.1972.6655.
[64] R.D. Shannon, Revised effective ionic radii and systematic studies of interatomic distances in halides and chalcogenides, Acta Crystallogr. Sect. A Cryst. Phys. Diffr. Theor. Gen. Crystallogr. 32 (1976) 751–767, https://doi.org/10.1107/S0567739476001551.
[65] A. Tymiński, T. Grzyb, Enhancement of the up-conversion luminescence in $LaVO_4$ nanomaterials by doping with M^{2+}, M^{4+} (M^{2+} = Sr^{2+}, Ba^{2+}, Mg^{2+}; M^{4+} = Sn^{4+}) ions, J. Alloys Compd. 782 (2019) 69–80, https://doi.org/10.1016/j.jallcom.2018.12.112.
[66] X. Chen, J. Ding, S. Yang, L. Zhou, H. Chen, A. Wu, L. Jiang, Sol–gel auto-combustion synthesis and luminescence properties of RVO_4: ln^{3+} (R= La, Gd; Ln= Sm, Er, Ho, Yb/Er) microcrystals, J. Mod. Opt. 67 (2020) 1078–1088, https://doi.org/10.1080/09500340.2020.1810348.
[67] D. Errandonea, A.B. Garg, Recent progress on the characterization of the high-pressure behaviour of AVO_4 orthovanadates, Prog. Mater. Sci. 97 (2018) 123–169, https://doi.org/10.1016/j.pmatsci.2018.04.004.
[68] J.E. Munoz-Santiuste, V. Lavin, U.R. Rodriguez-Mendoza, C. Ferrer-Roca, D. Errandonea, D. Martinez-Garcia, P. Rodriguez-Hernandez, A. Munoz, M. Bettinelli, Experimental and theoretical study on the optical properties of $LaVO_4$ crystals under pressure, Phys. Chem. Chem. Phys. 20 (2018) 27314–27328, https://doi.org/10.1039/C8CP04701D.
[69] D. Song, C. Guo, T. Li, Luminescence of the self-activated vanadate phosphors $Na_2LnMg_2V_3O_{12}$ (Ln = Y, Gd), Ceram. Int. 41 (2015) 6518–6524, https://doi.org/10.1016/j.ceramint.2015.01.094.
[70] A.K.R. Choudhury, Instrumental Colourant Formulation in Principles of Colour and Appearance Measurement, first ed., Woodhead Publishing, Cambridge, 2015.
[71] A. Escobedo Morales, E. Sanchez Mora, U. Pal, Use of diffuse reflectance spectroscopy for optical characterization of un-supported nanostructures, Rev. Mexic. Fisica S53 (2007) 18–22. http://www.redalyc.org/articulo.oa?id=57028299004.
[72] V. Panchal, D. Errandonea, A. Segura, P. Rodriguez-Hernandez, A. Munoz, S. Lopez-Moreno, M. Bettinelli, The electronic structure of zircon-type orthovanadates: effects of high-pressure and cation substitution, J. Appl. Phys. 110 (2011) 043723, https://doi.org/10.1063/1.3626060.
[73] G. Blasse, On the Eu^{3+} fluorescence of mixed metal oxides. IV. The photoluminescent efficiency of Eu^{3+} activated oxide, J. Chem. Phys. 45 (1966) 2356–2360, https://doi.org/10.1063/1.1727946.
[74] G. Blasse, B.C. Grabmaier, Luminescent Materials, Springer Berlin, Heidelberg, 1994.
[75] O. Chukova, S. Nedilko, S. Zayets, R. Boyko, P. Nagornyi, M. Slobodyanik, Luminescent spectroscopy of sodium titanium orthophosphate crystals doped with samarium and praseodymium ions, Opt. Mater. 30 (2008) 684–686, https://doi.org/10.1016/j.optmat.2007.02.008.
[76] Q. Lv, R. Deng, J. Guo, Z. Zhou, Z. Ma, X. Hu, W. Shi, B. Deng, Y. Yu, R. Yu, Abnormal thermal quenching and optical performance of new niobate perovskite $Sr_3LaNb_3O_{12}$:Sm^{3+} phosphors for w-LEDs, J. Lumin. 252 (2022) 119320, https://doi.org/10.1016/j.jlumin.2022.119320.
[77] P. Biswas, V. Kumar, N. Padha, H.C. Swart, Synthesis, structural and luminescence studies of $LiSrVO_4$:Sm^{3+} nanophosphor to fill amber gap in LEDs under n-U excitation, J. Mater. Sci. Mater. Electron. 28 (2017) 6159–6168, https://doi.org/10.1007/s10854-016-6294-3.